



THE UNIVERSITY *of* EDINBURGH

Edinburgh Research Explorer

Extensive crustal extraction in Earth's early history inferred from molybdenum isotopes

Citation for published version:

McCoy-West, AJ, Chowdhury, P, Burton, KW, Sossi, P, Nowell, GM, Fitton, J, Kerr, AC, Cawood, PA & Williams, HM 2019, 'Extensive crustal extraction in Earth's early history inferred from molybdenum isotopes', *Nature Geoscience*. <https://doi.org/10.1038/s41561-019-0451-2>

Digital Object Identifier (DOI):

[10.1038/s41561-019-0451-2](https://doi.org/10.1038/s41561-019-0451-2)

Link:

[Link to publication record in Edinburgh Research Explorer](#)

Document Version:

Peer reviewed version

Published In:

Nature Geoscience

General rights

Copyright for the publications made accessible via the Edinburgh Research Explorer is retained by the author(s) and / or other copyright owners and it is a condition of accessing these publications that users recognise and abide by the legal requirements associated with these rights.

Take down policy

The University of Edinburgh has made every reasonable effort to ensure that Edinburgh Research Explorer content complies with UK legislation. If you believe that the public display of this file breaches copyright please contact openaccess@ed.ac.uk providing details, and we will remove access to the work immediately and investigate your claim.



Extensive crustal extraction in Earth's early history inferred from molybdenum isotopes

Alex J. McCoy-West^{1, 2}, Priyadarshi Chowdhury², Kevin W. Burton¹, Paolo Sossi³, Geoff M. Nowell¹, J. Godfrey Fitton⁴, Andrew C. Kerr⁵, Peter A. Cawood² and Helen M. Williams^{1, 6}

¹Department of Earth Sciences, Durham University, Elvet Hill, Durham DH1 3LE, UK

²School of Earth, Atmosphere and Environment, Monash University, Clayton, Victoria, 3800, Australia

³Institute of Geochemistry and Petrology, ETH Zürich

⁴School of GeoSciences, University of Edinburgh, Edinburgh EH9 3FE, UK

⁵School of Earth and Ocean Sciences, Cardiff University, Park Place, Cardiff CF10 3AT, UK

⁶Department of Earth Sciences, University of Cambridge, Downing Street, Cambridge CB2 3EQ, UK

Number of words: 3,084

Number of references: 50

Number of figures: 4

First paragraph (words): 153

Caption Length (words): 100, 96, 64, 90

Methods number of words: 1,804

Corresponding Author

Alex McCoy-West (alex.mccoywest@monash.edu)

School of Earth, Atmosphere and Environment, Monash University, Clayton, Victoria, 3800, Australia

FIRST PARAGRAPH

Estimates of the volume of the earliest crust based on zircon ages and radiogenic isotopes remain equivocal. Stable isotope systems, such as molybdenum, have the potential to provide further constraints but remain underused, due to the lack of complementarity between mantle and crustal reservoirs. Here we present molybdenum isotope data for Archean komatiites and Phanerozoic komatiites and picrites and demonstrate that their mantle sources all possess sub-chondritic signatures complementary to the super-chondritic continental crust. These results confirm that the present-day degree of mantle depletion was achieved by 3.5 billion years ago and that the Earth has been in a steady state with respect to molybdenum recycling. Mass balance modelling shows that this early mantle depletion requires the extraction of a far greater volume of mafic-dominated proto-crust than previous thought, more than twice the volume of the continental crust today, implying rapid crustal growth and destruction in the first billion years of Earth's history.

14 MAIN TEXT

15 The nature, extent and geodynamic settings of crustal formation and recycling are poorly
16 constrained, particularly during Hadean-early Archean times for which the rock-record is
17 scarce^{1,2}. The growth of the crust is estimated to be either temporally skewed with >60-80% of
18 the present-day volume of continental crust (PVCC) forming by 3 billion years ago (Ga)²⁻⁵, or
19 much more gradual with time^{1,6}. These growth curves are derived either from zircon formation
20 ages^{1,2} or from radiogenic isotopic evolution within the crust-mantle system⁶⁻⁸. Zircon ages
21 provide the lower bound on crustal growth as they cannot constrain the magnitude of recycling.
22 In contrast, growth curves of radiogenic isotope systems track the evolution of mantle depletion
23 and implicitly consider both crust extraction and recycling^{3,9}. The complementarity of the
24 crustal and mantle reservoirs for long-lived radiogenic isotopes (Sr-Nd-Hf) has long been
25 established, with time-dependent models requiring that only ~25-50% of the mantle's mass
26 underwent melt extraction to balance the present-day compositions of the depleted mantle and
27 crust^{7,8,10}. Estimating crustal growth from a mantle-depletion perspective using time-invariant
28 proxies provides an alternative approach⁴. As stable isotope ratios are time-independent, they
29 fit this criteria and can be used to put quantitative constraints on differentiation processes
30 occurring in the early Earth. However, this approach is hindered by the lack of resolvable
31 isotopic variation in samples representative of the depleted mantle and crust for many non-
32 traditional stable isotope systems.

33 Molybdenum (Mo) stable isotopes ($\delta^{98}\text{Mo} = [({}^{98}\text{Mo}/{}^{95}\text{Mo}_{\text{sample}} / {}^{98}\text{Mo}/{}^{95}\text{Mo}_{\text{standard}}) - 1]$
34 $\times 1000$; with the standard NIST3134 = 0‰) may be an exception, with a picture emerging of
35 two complementary reservoirs in the crust and mantle. Chondritic meteorites, the purported
36 building blocks of the terrestrial planets, have a relatively homogeneous average $\delta^{98}\text{Mo}$ of
37 $-0.154 \pm 0.013\text{‰}$ ^{11,12} (all errors on averages herein are 95% standard errors). Estimates of the

composition of the modern continental crust based on molybdenites, granites and primitive arc-related basalts yield super-chondritic $\delta^{98}\text{Mo}$ values ranging from +0.05‰ to +0.3‰¹³⁻¹⁵. If the bulk Earth is chondritic with respect to Mo stable isotopes and Mo is not fractionated during its partitioning into Earth's core (cf. ¹⁶), then an isotopically light, sub-chondritic Mo reservoir must exist in the mantle^{17,18}. Arc lavas show extremely variable $\delta^{98}\text{Mo}$ (−0.88‰ to +0.24‰) but the consensus is that subduction zones appear to be fluxing isotopically light Mo into the mantle¹⁹⁻²¹. However, whether this material is efficiently recycled or has enough mass to affect the composition of the bulk mantle remains to be established. Previous Mo isotope analyses of Archean komatiites¹⁷ have slightly sub-chondritic compositions, but within error of chondrites¹¹, while five of the most depleted ($^{143}\text{Nd}/^{144}\text{Nd} > 0.5131$) mid-ocean ridge basalts (MORB) measured are resolvably sub-chondritic²². Therefore, it is possible that a complementary light sub-chondritic Mo isotope reservoir is present within the mantle¹⁸, but its composition and nature remains poorly constrained.

Here, we focus on komatiite and picrite samples from four well characterized suites: two from the Archean, the 3.5 Ga Komati (South Africa) and 2.7 Ga Munro (Canada) komatiites²³, and two from the Phanerozoic, the 89 Ma Gorgona (Colombia) komatiites²⁴ and the 61 Ma Baffin Island (NE Canada) picrites^{25,26}, to better constrain the Mo isotope composition of the mantle throughout Earth's history. The selection of rock samples for this purpose is non-trivial due to the complex behaviour of Mo during mantle melting. Although none of the major silicate phases in the mantle host significant Mo²⁷, Mo is chalcophile and the presence of residual sulfides will strongly affect the Mo concentration of a melt¹⁸. Furthermore, isotopic studies of Mo isotopes in ultramafic lithologies are hampered by the low concentrations of Mo (<50 ng/g) and the significant isotopic variability observed in mantle lithologies^{12,17}. The ultramafic lavas studied here formed at elevated temperatures (>1400 °C) by high-degrees of partial melting (>25%), which would have led to complete sulfide extraction

from their source regions²⁸, such that their Mo isotope compositions should closely resemble that of their mantle source regions. Our new results for these samples combined with existing data are used to constrain the $\delta^{98}\text{Mo}$ of the Earth's mantle, and subsequently global crustal volumes, during Hadean-Archean times.

ESTABLISHING A SUB-CHONDRITIC MO ISOTOPE RESERVIOR

Our measurements show sub-chondritic values for unaltered Archean Komati and Munro komatiites with $\delta^{98}\text{Mo}$ varying from -0.22 to -0.18‰ (Fig. 1; Table S1). Previous analyses of Archean komatiites presented in Greber et al.¹⁷ define a wide range ($-0.32\text{‰} < \delta^{98}\text{Mo} < +0.07\text{‰}$) with an average $\delta^{98}\text{Mo}$ of the four investigated localities calculated as $-0.210 \pm 0.098\text{‰}$. Combining these results is not straightforward. For example, previously analysed samples from the Vetreny Belt, Fennoscandia have experienced significant crustal assimilation²⁹ and consequently display resolvable heavier $\delta^{98}\text{Mo}$ ($-0.077 \pm 0.083\text{‰}$). We thus disregard these samples in subsequent interpretations. In Greber et al.¹⁷, lavas from the Komati Formation that were undoubtedly modified by alteration were excluded (Fig. 1; $\delta^{98}\text{Mo}$ up to $+0.44\text{‰}$), but no further filtering for alteration was attempted. Given the high mobility of Mo in fluids at low temperatures³⁰, we have filtered the Archean komatiite Mo isotope data (Fig. S1), excluding samples that display major element mobility unrelated to magmatic differentiation and are thus considered to have been modified by alteration (see supplement). Our new data, along with the alteration-filtered dataset of¹⁷, allows the calculation of the $\delta^{98}\text{Mo}$ of Archean komatiites as $-0.199 \pm 0.019\text{‰}$.

Samples from the Phanerozoic Gorgona komatiites, the youngest komatiite occurrence in the world, have a restricted range of $\delta^{98}\text{Mo}$ from -0.18 to -0.25‰ and yield an average $\delta^{98}\text{Mo}$ of $-0.207 \pm 0.034\text{‰}$, within error of their Archean equivalents. In contrast, the

Phanerozoic Baffin Island picrites possess variable $\delta^{98}\text{Mo}$ from -0.13 to -0.32‰ , which at first glance suggests a lighter mantle $\delta^{98}\text{Mo}$ (Fig. 1). However, the Baffin Island picrites represent a special case of disequilibrium olivine accumulation²⁶ and after this is corrected the composition of the parental melt is calculated as $\delta^{98}\text{Mo} = -0.210 \pm 0.010\text{‰}$ (Table S2; Figs. S3-5), within error of depleted MORB²², the Gorgona komatiites, and three Archean komatiite localities that span 800 Ma. These data thus demonstrate that the Mo isotope composition of the accessible mantle has changed little over the last 3.5 Ga. The data for magmatic rocks are further augmented by mantle xenoliths enabling us to calculate the average composition of the depleted mantle as $\delta^{98}\text{Mo} = -0.204 \pm 0.008\text{‰}$ (Table S3).

These results place several new constraints on the evolution of Earth's mantle, notably:

- 1) the Mo isotope composition of the accessible mantle is unambiguously sub-chondritic (an analysis of variance test confirms that the mantle samples are a resolvably different population to chondritic meteorites at the 99% significance level; $p\text{-value} < 0.001$);
- 2) the formation of this reservoir must have occurred before ~ 3.5 Ga;
- 3) it must have had a substantial volume (magmas generated at a range of melting depths are affected); and
- 4) no resolvable temporal variations are observed with Archean komatiites ranging in age from 3.5–2.7 Ga having identical $\delta^{98}\text{Mo}$ to Cretaceous Gorgona komatiites, Paleogene Baffin Island picrites and modern MORB (an analysis of variance test confirms that the means of these populations are identical; $p\text{-value} \sim 0.42$).

Together these constraints demonstrate that from a Mo isotope perspective most of the present-day depletion of the mantle must have been completed by the Paleoarchean. This finding is in agreement with independent constraints on the temporal chemical evolution of continental basalts, which indicates a nearly constant amount of mantle depletion since ~ 3.8 Ga³¹. However, the amount of mantle depletion, and hence the volume of early continental crust produced and subsequently destroyed, remain under-constrained^{3,9}. Nonetheless, most studies agree that 30–50% melt depletion of the whole mantle can reproduce most of the

radiogenic and incompatible element signatures of the crust and depleted mantle, assuming they represent complementary reservoirs^{7,8,10}. This has significant implications for the growth of early crust given that the proto-crust and depleted mantle should chemically complement each other, if no other processes have perturbed the system. We explore this further below.

COMPOSITION OF THE SILICATE EARTH

Due to the refractory nature of Mo in the solar nebula, we assume that the proto-Earth inherited the $\delta^{98}\text{Mo}$ of chondritic meteorites (Fig. 2). Soon after accretion, core formation occurred ($\approx 34 \text{ Ma}^{32}$) resulting in the efficient removal of the highly siderophile elements into the Fe-Ni metal core, including 95% of the Earth's original Mo^{33} (Table S5). The near quantitative removal of Mo to the core means isotope ratios in the metallic phase are unlikely to be fractionated from those in bulk chondrites, as observed in iron meteorites¹¹. Early experimental work suggested this sequestration of Mo may have been associated with a small but resolvable isotopic fractionation of the silicate portion of the planet³⁴. However, recent metal-silicate experiments which incorporate the effect of Mo valence state¹⁶ suggest a significantly reduced $\Delta^{98}\text{Mo}_{\text{metal-silicate}}$ of as little as -0.008‰ (assuming $\text{Mo}^{6+}/\Sigma\text{Mo} = 0.1$; $T = 2500 \text{ °C}$), which means the mantle would remain within the error of the composition of chondrites following core formation. Subsequent modification of the residual bulk silicate Earth (BSE) may have occurred during: 1) the Moon-forming impact: where a planet-sized body impacted Earth and added volatiles, including significant sulfur, which may have been sequestered to the outer core in the “Hadean matte” ($<1\%$ of core mass; this sulfide-enriched phase is expected to have preferentially incorporated isotopically light $\text{Mo}^{35,36}$); or 2) late accretion: since geochemical modelling suggests that all of the Mo in Earth's mantle was added during the last 10% of accretion³⁷, with N -body simulations require only $\sim 1\%$ of the Earth's mass was accreted following the Moon-forming impact³⁸. Ultimately, due to the chondritic composition of the

new materials these processes will not significantly change the $\delta^{98}\text{Mo}$ of the BSE, which should be around $\delta^{98}\text{Mo} \approx -0.154\text{‰}$. Therefore, the only remaining global-scale mechanism that can modify the Earth's Mo isotope budget and account for the Earth's super-chondritic crust and sub-chondritic mantle is the extraction of the crust (Fig. 2). Furthermore, the presence of positive Nb anomalies and radiogenic Nd isotope compositions in some komatiite suites suggest that their source regions have previously undergone melt extraction^{23,39}.

EXTRACTION OF AN ISOTOPICALLY HEAVY CRUST

The sub-chondritic mantle $\delta^{98}\text{Mo}$ signature may be the result of partial melting²² or continental crust extraction¹⁷ or both, but the exact magnitude of fractionation remains uncertain. Here we have developed a partial melting model to assess the direction and magnitude of fractionation of $\delta^{98}\text{Mo}$ between melt and residual mantle (Fig. 3). This modelling demonstrates several important points: 1) high-MgO partial melts are accurate recorders of the Mo isotope composition of their mantle sources, because at high temperatures $\Delta^{98}\text{Mo}_{\text{melt-solid}} < 0.012\text{‰}$ at 30% melting (Fig. 3a); 2) melting of a chondritic reservoir to form basalt reproduces the average basalt used in modelling ($\delta^{98}\text{Mo} = -0.10\text{‰}$) with ~12% melting at 1300 °C. This ~0.05‰ difference in $\delta^{98}\text{Mo}$ is comparable to that observed between N-MORB²² and the depleted mantle composition (herein); 3) the composition of modern upper continental crust or Phanerozoic granites (Fig. 1; $\Delta^{98}\text{Mo}_{\text{granite-mantle}} + 0.36\text{‰}$) cannot be generated by direct melting of the mantle. The majority of the enrichment of these samples in heavy $\delta^{98}\text{Mo}$ must instead result from intracrustal differentiation, either through the addition of isotopically heavy subduction zone fluids¹⁹ or hydrothermal fluids⁴⁰ or the removal of isotopically light hydrous phases (biotite or amphibole)¹³ into cumulates in the lower crust.

Molybdenum isotope fractionation during melt extraction may be driven by both changes in Mo oxidation state and co-ordination number. Given that Mo^{6+} is significantly more

incompatible²⁷ than Mo⁴⁺, residues of melting will have lower Mo⁶⁺/ΣMo than melt in addition to higher mean co-ordination number, and hence will display lighter δ⁹⁸Mo consistent with the sense of fractionation observed in the komatiites measured here (Fig. 1). The oxidation state of Mo in the modern mantle remains uncertain, however; partitioning studies indicate Mo is predominantly hexavalent in melts at typical upper mantle conditions (Mo⁶⁺/ΣMo ≈ 0.99^{16,27,41}). Although mantle oxygen fugacity is generally considered to have been constant for the last ~3.5 Ga⁴², recent work using V partitioning provides strong evidence of increasing oxygen fugacity with time⁴³, therefore here we impose Mo⁶⁺/ΣMo = 0.95 for early mantle melting (Fig. 3b). Creation of felsic components of the Hadean-Eoarchean crust such as tonalite-trondhjemite-granodiorite (TTG) granitoids, requires remelting of metabasalt (mafic amphibolite)⁴⁴, which will further enrich this felsic component in heavier isotopes by up to 0.08‰ (at 900 °C and F = 20%), but cannot explain the full range of heavy δ⁹⁸Mo observed. The models presented here evaluate mantle melting only and should be considered minimum estimates and approximate until Mo isotope fractionation factors can be independently determined for accessory phases that may retain isotopically light Mo (e.g. garnet, amphibole, sulfide, rutile). Nonetheless, they demonstrate that there is no need to invoke subduction zone processes in the early Earth to form the mafic crusts discussed below, which can instead be generated solely through mantle melting processes.

EXTENSIVE EXTRACTION AND RECYCLING OF EARLY CRUST

Assuming a two-reservoir model involving a proto-crust(C) and depleted mantle (DM), we have estimated the crustal volume that is required to have formed by ~3.5 Ga to reconcile the δ⁹⁸Mo and Mo-concentration of the mantle that sourced the Archean komatiites using the mass-balance equation:

$$m_c = \frac{m_{DM} \cdot [Mo]_{DM} \cdot (\delta_{BSE}^{98} - \delta_{DM}^{98})}{[Mo]_c \cdot (\delta_c^{98} - \delta_{BSE}^{98})}$$

where m_i , $[Mo]_i$ and δ_i^{98} represents the mass, Mo concentration and Mo isotope composition, respectively, of the various reservoirs. It is important to note the mass balance modelling presented here does not reflect the instantaneous removal of melts from the mantle, but rather the effect of the time-integrated isolation of the proto-crust from the convecting mantle.

Calculations of continental growth based on the zircon archive and mantle depletion commonly use the present-day continental crust as the crustal endmember. However, there are two major compositional differences between the early continents and their modern analogues^{2,8}. These are: 1) TTG granitoids were the dominant felsic rocks with true potassic (K) granites subordinate in abundance⁴⁴ and, 2) mafic lithologies were more abundant than their felsic counterparts^{45,46}. Here we assume the BSE had an initial $\delta^{98}\text{Mo}$ equal to chondritic meteorites (for alternate scenarios see Fig. S6) and we investigate two scenarios encompassing the variability of $\delta^{98}\text{Mo}$ in Archean felsic rocks (granites or TTGs represent the felsic endmember; Fig. 4). These scenarios thus provide the minimum and maximum estimates of the extent of pre-3.5 Ga crust extraction. We then calculate crustal volumes for three different model proto-crusts: a hypothetical purely felsic crust, Mafic crust-A (minimum based on a mafic crust) and Mafic crust-B (a likely Eoarchean crustal composition). Calculations based on the purely felsic crusts suggest a minimum of 0.5-1.5 times the PVCC ($\sim 7.2 \times 10^9 \text{ km}^3$) existed prior to 3.5 Ga based on 30 % depletion of the whole mantle (Fig. 4). This range is consistent with the growth model calculated using Nb/U ratios of the crust-mantle system⁴, but is higher than those calculated using the crustal zircon formation ages (<50% of PVCC at 3.5 Ga;²). This suggests that time-invariant proxies of mantle depletion record similar volumes of early crust extraction, whereas their difference with the zircon-based models reflects the

influence of crustal recycling. More realistic calculations based on dominantly mafic crust types require crustal volumes greater than the PVCC by ~3.5 Ga (Fig 4). For example, in the preferred Eoarchean scenario with a TTG felsic component the crustal volumes based on Mafic crust-A and -B will be 2.5 and 3.8 times the PVCC, respectively, assuming the minimum likely amount of mantle depletion (30%; ^{7,8,10}; Fig. 4b). These higher values are mostly a consequence of the lower Mo concentration (and to a minor extent the lighter isotopic compositions) of these model crusts (see Table S5). It is debatable whether to consider dominantly mafic crust as continental or not^{45,46}, but our calculations show that even the volume of a hypothetical TTG crust would have been greater than the PVCC, provided the depleted mantle size exceeds ~20% of the whole mantle. Thus, it is highly likely that a greater volume of crust than the PVCC was extracted in the first billion years of Earth's history, most of which was then subsequently recycled into the mantle.

Large-scale crust extraction is consistent with the prediction of voluminous melting of the mantle owing to its hotter thermal structure during Hadean-Archean times⁴⁷. However, our calculated crustal volumes represent the amount of crust extracted from the mantle and not its net growth, which is determined by the difference between extracted (generated) and recycled volumes of the crust⁹. Nevertheless, high rates of crust formation should result in rapid crustal growth unless the recycling rates equal or exceed extraction rates. Several independent continental growth models^{2,3,5} do suggest extremely rapid continental growth consistent with the idea that extensive crust formation may have happened on the early Earth. Given the dearth of such old rocks in the present rock record, it is unequivocal that much of the >3.5 Ga crust has been recycled. Mantle-derived isotopic heterogeneities are widespread in modern basalts, reflecting sluggish mantle mixing. Modelling of stagnant lid tectonic regimes, which may have operated early in Earth history, shows that mixing was up to an order of magnitude slower under these conditions⁴⁸ therefore it is expected that this recycled crustal material will not have

231 mixed back completely into the accessible mantle. Although difficult to constrain, recent
232 studies on Archean continental recycling^{49,50} suggest extensive recycling (but not exceeding
233 the formation rates) of the crust, with a volume equivalent to the PVCC probably recycled
234 during the late Archean⁴⁹. If the recycling rates were similar during most of the Hadean-
235 Archean, twice the PVCC could have been recycled back into the mantle during that period.
236 Consequently, we have not only been significantly underestimating the volumes of early
237 formed crust, but also the amount of material that was being recycled back into the mantle.

Accepted Manuscript

Acknowledgements

Dave Selby is thanked for access to carius tube facilities. This project was funded by a European Research Council Starting Grant (“HabitablePlanet” 306655) to HMW and a NERC Grant (NE/M0003/1) to KWB. While at Monash AMW, PC and PAC were supported by ARC grant FL160100168.

Author Contributions

AMW, KWB and HMW conceived the study. AMW undertook the chemistry and mass spectrometry with assistance from GMN. JGF, ACK and PS provided the samples. AMW and PC developed the mass balance modelling. AMW and PS developed the Mo isotope partial melting model. AMW wrote the paper, while all the authors contributed to discussions on early crustal volumes and editing the paper.

Financial and non-financial competing interests

The authors declare no competing financial interests.

Figure Captions

Figure 1: Variation of $\delta^{98}\text{Mo}$ in komatiites, picrites and major mantle and crustal reservoirs. Filled symbols are data analysed herein with hollow symbols data taken from Greber et al.¹⁷. All individual analyses are plotted with the 2 standard deviation long term error, with the shaded areas for different formations and reservoirs the being 95% standard errors. The dark grey band represents chondritic meteorites ($\delta^{98}\text{Mo} = -0.154 \pm 0.013\text{‰}$; ^{11,12}) with the green bar representing the resolvable lighter depleted mantle ($\delta^{98}\text{Mo} = -0.204 \pm 0.008\text{‰}$; herein). Average Archean komatiites ($\delta^{98}\text{Mo} = -0.199 \pm 0.019\text{‰}$; herein) with other reservoirs from ^{12,14,22} (see Table S3).

Figure 2: Schematic Mo evolution of Earth's mantle and crust during planetary differentiation. Earth accretes from chondritic meteorites thus the bulk Earth initial $\delta^{98}\text{Mo}$ will be chondritic. During core formation 95 % of Earth's Mo is sequestered into the core trapping isotopically light Mo in the metal phase, possibly making the residual BSE heavier. Subsequent extraction of Earth's isotopically heavy crust prior to 3.5 Ga resulted in a bulk mantle that is lighter than the building blocks of Earth. Earth's earliest crust was more mafic than modern crust and therefore had a different Mo concentration and isotopic composition.

Figure 3: Partial melting model showing that the degree of enrichment of heavy Mo isotopes in the melt phase is controlled by both temperature and the valance state of Mo. (a) the effect of varying temperature at a constant oxygen fugacity ($\text{Mo}^{6+}/\Sigma\text{Mo} = 0.95$). Shaded areas represent varying the temperature by $\pm 100^\circ\text{C}$. (b) The effect of varying oxygen fugacity at a constant temperature (1300°C).

Figure 4: Results of Mo isotope mass balance calculations which estimate the mass of crust extraction required to balance the composition of the depleted mantle. This mass of crust can then be converted into a volume of crust (V_C) relative to the present volume of continental crust (V_{PCC}) and varies depending on the proportion of the total BSE that has undergone melt depletion ($M_{\text{DM}}/M_{\text{BSE}}$). Mafic crust-A and -B contain mafic and felsic rocks in 50:50 and 75:25 ratios, respectively. The shaded areas represent varying the proportions of the two endmembers by $\pm 5\%$.

285 REFERENCES

- 286 1 Condie, K. C. Episodic continental growth and supercontinents: a mantle avalanche connection? *Earth*
287 *and Planetary Science Letters* **163**, 97-108 (1998).
- 288 2 Dhuime, B., Hawkesworth, C. J., Cawood, P. A. & Storey, C. D. A change in the geodynamics of
289 continental growth 3 billion years ago. *Science* **335**, 1334-1336, doi:10.1126/science.1216066 (2012).
- 290 3 Korenaga, J. Estimating the formation age distribution of continental crust by unmixing zircon ages.
291 *Earth and Planetary Science Letters* **482**, 388-395, doi:<https://doi.org/10.1016/j.epsl.2017.11.039>
292 (2018).
- 293 4 Campbell, I. H. Constraints on continental growth models from Nb/U ratios in the 3.5 Ga Barberton
294 and other Archaean basalt-komatiite suites. *American Journal of Science* **303**, 319-351,
295 doi:10.2475/ajs.303.4.319 (2003).
- 296 5 Armstrong, R. L. Radiogenic isotopes: the case for crustal recycling on a near-steady-state no-
297 continental-growth Earth. *Philosophical Transactions of the Royal Society of London* **301**, 443-472,
298 doi:10.1098/rsta.1981.0122 (1981).
- 299 6 McCulloch, M. T. & Bennett, V. C. Progressive growth of the Earth's continental crust and depleted
300 mantle: Geochemical constraints. *Geochimica et Cosmochimica Acta* **58**, 4717-4738,
301 doi:[http://dx.doi.org/10.1016/0016-7037\(94\)90203-8](http://dx.doi.org/10.1016/0016-7037(94)90203-8) (1994).
- 302 7 DePaolo, D. J. Crustal growth and mantle evolution: inferences from models of element transport and
303 Nd and Sr isotopes. *Geochimica et Cosmochimica Acta* **44**, 1185-1196,
304 doi:[https://doi.org/10.1016/0016-7037\(80\)90072-1](https://doi.org/10.1016/0016-7037(80)90072-1) (1980).
- 305 8 Jacobsen, S. B. Isotopic and chemical constraints on mantle-crust evolution. *Geochimica et*
306 *Cosmochimica Acta* **52**, 1341-1350, doi:[https://doi.org/10.1016/0016-7037\(88\)90205-0](https://doi.org/10.1016/0016-7037(88)90205-0) (1988).
- 307 9 Cawood, P. A., Hawkesworth, C. J. & Dhuime, B. The continental record and the generation of
308 continental crust. *GSA Bulletin* **125**, 14-32, doi:10.1130/B30722.1 (2013).
- 309 10 O'Nions, R. K., Evensen, N. M. & Hamilton, P. J. Geochemical modeling of mantle differentiation and
310 crustal growth. *Journal of Geophysical Research: Solid Earth* **84**, 6091-6101,
311 doi:10.1029/JB084iB11p06091 (1979).
- 312 11 Burkhardt, C., Hin, R. C., Kleine, T. & Bourdon, B. Evidence for Mo isotope fractionation in the solar
313 nebula and during planetary differentiation. *Earth and Planetary Science Letters* **391**, 201-211,
314 doi:<http://dx.doi.org/10.1016/j.epsl.2014.01.037> (2014).
- 315 12 Liang, Y.-H. *et al.* Molybdenum isotope fractionation in the mantle. *Geochimica et Cosmochimica*
316 *Acta* **199**, 91-111, doi:<https://doi.org/10.1016/j.gca.2016.11.023> (2017).
- 317 13 Voegelin, A. R., Pettke, T., Greber, N. D., von Niederhäusern, B. & Nägler, T. F. Magma
318 differentiation fractionates Mo isotope ratios: Evidence from the Kos Plateau Tuff (Aegean Arc).
319 *Lithos* **190-191**, 440-448, doi:<http://dx.doi.org/10.1016/j.lithos.2013.12.016> (2014).
- 320 14 Yang, J. *et al.* The molybdenum isotopic compositions of I-, S- and A-type granitic suites. *Geochimica*
321 *et Cosmochimica Acta* **205**, 168-186, doi:<https://doi.org/10.1016/j.gca.2017.01.027> (2017).
- 322 15 Greber, N. D., Pettke, T. & Nägler, T. F. Magmatic-hydrothermal molybdenum isotope fractionation
323 and its relevance to the igneous crustal signature. *Lithos* **190-191**, 104-110,
324 doi:<https://doi.org/10.1016/j.lithos.2013.11.006> (2014).
- 325 16 Hin, R. C., Burnham, A. D., Gianolio, D., Walter, M. J. & Elliott, T. Molybdenum isotope fractionation
326 between Mo⁴⁺ and Mo⁶⁺ in silicate liquid and metallic Mo. *Chemical Geology* **504**, 177-189,
327 doi:<https://doi.org/10.1016/j.chemgeo.2018.11.014> (2019).
- 328 17 Greber, N. D., Puchtel, I. S., Nägler, T. F. & Mezger, K. Komatiites constrain molybdenum isotope
329 composition of the Earth's mantle. *Earth and Planetary Science Letters* **421**, 129-138,
330 doi:<https://doi.org/10.1016/j.epsl.2015.03.051> (2015).
- 331 18 Willbold, M. & Elliott, T. Molybdenum isotope variations in magmatic rocks. *Chemical Geology* **449**,
332 253-268, doi:<https://doi.org/10.1016/j.chemgeo.2016.12.011> (2017).
- 333 19 Freymuth, H., Vils, F., Willbold, M., Taylor, R. N. & Elliott, T. Molybdenum mobility and isotopic
334 fractionation during subduction at the Mariana arc. *Earth and Planetary Science Letters* **432**, 176-186,
335 doi:<http://dx.doi.org/10.1016/j.epsl.2015.10.006> (2015).
- 336 20 Gaschnig, R. M. *et al.* The Molybdenum Isotope System as a Tracer of Slab Input in Subduction
337 Zones: An Example From Martinique, Lesser Antilles Arc. *Geochemistry, Geophysics, Geosystems* **18**,
338 4674-4689, doi:10.1002/2017GC007085 (2017).
- 339 21 König, S., Wille, M., Voegelin, A. & Schoenberg, R. Molybdenum isotope systematics in subduction
340 zones. *Earth and Planetary Science Letters* **447**, 95-102, doi:<https://doi.org/10.1016/j.epsl.2016.04.033>
341 (2016).
- 342 22 Bezard, R., Fischer-Gödde, M., Hamelin, C., Brennecke, G. A. & Kleine, T. The effects of magmatic
343 processes and crustal recycling on the molybdenum stable isotopic composition of Mid-Ocean Ridge

- Basalts. *Earth and Planetary Science Letters* **453**, 171-181, doi:<http://dx.doi.org/10.1016/j.epsl.2016.07.056> (2016).
- 23 Sossi, P. A. *et al.* Petrogenesis and Geochemistry of Archean Komatiites. *Journal of Petrology* **57**, 147-184, doi:10.1093/petrology/egw004 (2016).
- 24 Kerr, A. C. *et al.* The petrogenesis of Gorgona komatiites, picrites and basalts: new field, petrographic and geochemical constraints. *Lithos* **37**, 245-260, doi:[http://dx.doi.org/10.1016/0024-4937\(95\)00039-9](http://dx.doi.org/10.1016/0024-4937(95)00039-9) (1996).
- 25 Starkey, N. A. *et al.* Helium isotopes in early Iceland plume picrites: Constraints on the composition of high ³He/⁴He mantle. *Earth and Planetary Science Letters* **277**, 91-100, doi:<https://doi.org/10.1016/j.epsl.2008.10.007> (2009).
- 26 McCoy-West, A. J., Godfrey Fitton, J., Pons, M.-L., Inglis, E. C. & Williams, H. M. The Fe and Zn isotope composition of deep mantle source regions: Insights from Baffin Island picrites. *Geochimica et Cosmochimica Acta* **238**, 542-562, doi:<https://doi.org/10.1016/j.gca.2018.07.021> (2018).
- 27 Leitzke, F. P. *et al.* Redox dependent behaviour of molybdenum during magmatic processes in the terrestrial and lunar mantle: Implications for the Mo/W of the bulk silicate Moon. *Earth and Planetary Science Letters* **474**, 503-515, doi:<https://doi.org/10.1016/j.epsl.2017.07.009> (2017).
- 28 McCoy-West, A. J., Bennett, V. C., O'Neill, H. S. C., Hermann, J. & Puchtel, I. S. The interplay between melting, refertilization and carbonatite metasomatism in off-cratonic lithospheric mantle under Zealandia: An integrated major, trace and platinum group element study. *Journal of Petrology* **56**, 563-604, doi:10.1093/petrology/egv011 (2015).
- 29 Puchtel, I. S. *et al.* Petrology of a 2.41 Ga remarkably fresh komatiitic basalt lava lake in Lion Hills, central Vetryny Belt, Baltic Shield. *Contributions to Mineralogy and Petrology* **124**, 273-290, doi:10.1007/s004100050191 (1996).
- 30 Keppler, H. & Wyllie, P. J. Partitioning of Cu, Sn, Mo, W, U, and Th between melt and aqueous fluid in the systems haplogranite-H₂O-HCl and haplogranite-H₂O-HF. *Contributions to Mineralogy and Petrology* **109**, 139-150, doi:10.1007/bf00306474 (1991).
- 31 Keller, B. & Schoene, B. Plate tectonics and continental basaltic geochemistry throughout Earth history. *Earth and Planetary Science Letters* **481**, 290-304, doi:<https://doi.org/10.1016/j.epsl.2017.10.031> (2018).
- 32 Kleine, T. & Walker, R. J. Tungsten Isotopes in Planets. *Annual Review of Earth and Planetary Sciences* **45**, 389-417, doi:10.1146/annurev-earth-063016-020037 (2017).
- 33 McDonough, W. F. in *Treatise on Geochemistry (First Edition)* Vol. 2 (eds Heinrich D. Holland & Karl K. Turekian) 547-568 (Elsevier, 2003).
- 34 Hin, R. C., Burkhardt, C., Schmidt, M. W., Bourdon, B. & Kleine, T. Experimental evidence for Mo isotope fractionation between metal and silicate liquids. *Earth and Planetary Science Letters* **379**, 38-48, doi:<http://dx.doi.org/10.1016/j.epsl.2013.08.003> (2013).
- 35 Savage, P. S. *et al.* Copper isotope evidence for large-scale sulphide fractionation during Earth's differentiation. *Geochemical Perspectives Letters* **1**, 53-64, doi:<http://dx.doi.org/10.7185/geochemlet.1506> (2015).
- 36 McCoy-West, A. J., Millet, M.-A. & Burton, K. W. The neodymium stable isotope composition of the silicate Earth and chondrites. *Earth and Planetary Science Letters* **480**, 121-132, doi:<https://doi.org/10.1016/j.epsl.2017.10.004> (2017).
- 37 Dauphas, N. The isotopic nature of the Earth's accreting material through time. *Nature* **541**, 521, doi:10.1038/nature20830 <https://www.nature.com/articles/nature20830#supplementary-information> (2017).
- 38 Jacobson, S. A. *et al.* Highly siderophile elements in Earth's mantle as a clock for the Moon-forming impact. *Nature* **508**, 84, doi:10.1038/nature13172 (2014).
- 39 Jahn, B.-M., Gruau, G. & Glikson, A. Y. Komatiites of the Onverwacht Group, S. Africa: REE geochemistry, Sm/Nd age and mantle evolution. *Contributions to Mineralogy and Petrology* **80**, 25-40, doi:10.1007/BF00376732 (1982).
- 40 Neely, R. A. *et al.* Molybdenum isotope behaviour in groundwaters and terrestrial hydrothermal systems, Iceland. *Earth and Planetary Science Letters* **486**, 108-118, doi:<https://doi.org/10.1016/j.epsl.2017.11.053> (2018).
- 41 O'Neill, H. S. C. & Eggins, S. M. The effect of melt composition on trace element partitioning: an experimental investigation of the activity coefficients of FeO, NiO, CoO, MoO₂ and MoO₃ in silicate melts. *Chemical Geology* **186**, 151-181, doi:[http://dx.doi.org/10.1016/S0009-2541\(01\)00414-4](http://dx.doi.org/10.1016/S0009-2541(01)00414-4) (2002).
- 42 Hibbert, K. E. J., Williams, H. M., Kerr, A. C. & Puchtel, I. S. Iron isotopes in ancient and modern komatiites: Evidence in support of an oxidised mantle from Archean to present. *Earth and Planetary Science Letters* **321-322**, 198-207, doi:<http://dx.doi.org/10.1016/j.epsl.2012.01.011> (2012).

- 43 Nicklas, R. W. *et al.* Secular mantle oxidation across the Archean-Proterozoic boundary: Evidence from V partitioning in komatiites and picrites. *Geochimica et Cosmochimica Acta* **250**, 49-75, doi:<https://doi.org/10.1016/j.gca.2019.01.037> (2019).
- 44 Moyen, J.-F. & Laurent, O. Archean tectonic systems: A view from igneous rocks. *Lithos* **302-303**, 99-125, doi:<https://doi.org/10.1016/j.lithos.2017.11.038> (2018).
- 45 Dhuime, B., Wuestefeld, A. & Hawkesworth, C. J. Emergence of modern continental crust about 3 billion years ago. *Nature Geoscience* **8**, 552, doi:10.1038/ngeo2466
<https://www.nature.com/articles/ngeo2466#supplementary-information> (2015).
- 46 Tang, M., Chen, K. & Rudnick, R. L. Archean upper crust transition from mafic to felsic marks the onset of plate tectonics. *Science* **351**, 372-375, doi:10.1126/science.aad5513 (2016).
- 47 Herzberg, C., Condie, K. & Korenaga, J. Thermal history of the Earth and its petrological expression. *Earth and Planetary Science Letters* **292**, 79-88, doi:<https://doi.org/10.1016/j.epsl.2010.01.022> (2010).
- 48 O'Neill, C., Debaille, V. & Griffin, W. Deep earth recycling in the Hadean and constraints on surface tectonics. *American Journal of Science* **313**, 912-932, doi:10.2475/09.2013.04 (2013).
- 49 Chowdhury, P., Gerya, T. & Chakraborty, S. Emergence of silicic continents as the lower crust peels off on a hot plate-tectonic Earth. *Nature Geoscience* **10**, 698, doi:10.1038/ngeo3010
<https://www.nature.com/articles/ngeo3010#supplementary-information> (2017).
- 50 Johnson, T. E., Brown, M., Kaus, B. J. P. & VanTongeren, J. A. Delamination and recycling of Archean crust caused by gravitational instabilities. *Nature Geoscience* **7**, 47, doi:10.1038/ngeo2019
<https://www.nature.com/articles/ngeo2019#supplementary-information> (2013).
- 51 Kerr, A. C. La Isla de Gorgona, Colombia: A petrological enigma? *Lithos* **84**, 77-101, doi:<http://dx.doi.org/10.1016/j.lithos.2005.02.006> (2005).
- 52 Rudge, J. F., Reynolds, B. C. & Bourdon, B. The double spike toolbox. *Chemical Geology* **265**, 420-431, doi:<http://dx.doi.org/10.1016/j.chemgeo.2009.05.010> (2009).
- 53 Willbold, M. *et al.* High-Precision Mass-Dependent Molybdenum Isotope Variations in Magmatic Rocks Determined by Double-Spike MC-ICP-MS. *Geostandards and Geoanalytical Research* **40**, 389-403, doi:10.1111/j.1751-908X.2015.00388.x (2016).
- 54 Greber, N. D., Siebert, C., Nägler, T. F. & Pettke, T. 898/95Mo values and Molybdenum Concentration Data for NIST SRM 610, 612 and 3134: Towards a Common Protocol for Reporting Mo Data. *Geostandards and Geoanalytical Research* **36**, 291-300, doi:10.1111/j.1751-908X.2012.00160.x (2012).
- 55 Goldberg, T. *et al.* Resolution of inter-laboratory discrepancies in Mo isotope data: An intercalibration. *Journal of Analytical Atomic Spectrometry* **28**, 724-735, doi:10.1039/C3JA30375F (2013).
- 56 Creech, J. B. & Paul, B. IsoSpike: Improved Double-Spike Inversion Software. *Geostandards and Geoanalytical Research* **39**, 7-15, doi:10.1111/j.1751-908X.2014.00276.x (2015).
- 57 Paton, C., Hellstrom, J., Paul, B., Woodhead, J. & Hergt, J. Iolite: Freeware for the visualisation and processing of mass spectrometric data. *Journal of Analytical Atomic Spectrometry* **26**, 2508-2518 (2011).
- 58 Li, Y. *et al.* Controlling Mechanisms for Molybdenum Isotope Fractionation in Porphyry Deposits: The Qulong Example. *Economic Geology* **114**, 981-992, doi:10.5382/econgeo.4653 (2019).
- 59 Zhao, P.-P. *et al.* Molybdenum Mass Fractions and Isotopic Compositions of International Geological Reference Materials. *Geostandards and Geoanalytical Research* **40**, 217-226, doi:10.1111/j.1751-908X.2015.00373.x (2015).
- 60 Yang, J. *et al.* Absence of molybdenum isotope fractionation during magmatic differentiation at Hekla volcano, Iceland. *Geochimica et Cosmochimica Acta* **162**, 126-136, doi:<http://dx.doi.org/10.1016/j.gca.2015.04.011> (2015).
- 61 Jacobsen, S. B. & Wasserburg, G. J. The mean age of mantle and crustal reservoirs. *Journal of Geophysical Research: Solid Earth* **84**, 7411-7427, doi:10.1029/JB084iB13p07411 (1979).
- 62 Hofmann, A. W. Mantle geochemistry: the message from oceanic volcanism. *Nature* **385**, 219, doi:10.1038/385219a0 (1997).

Figures

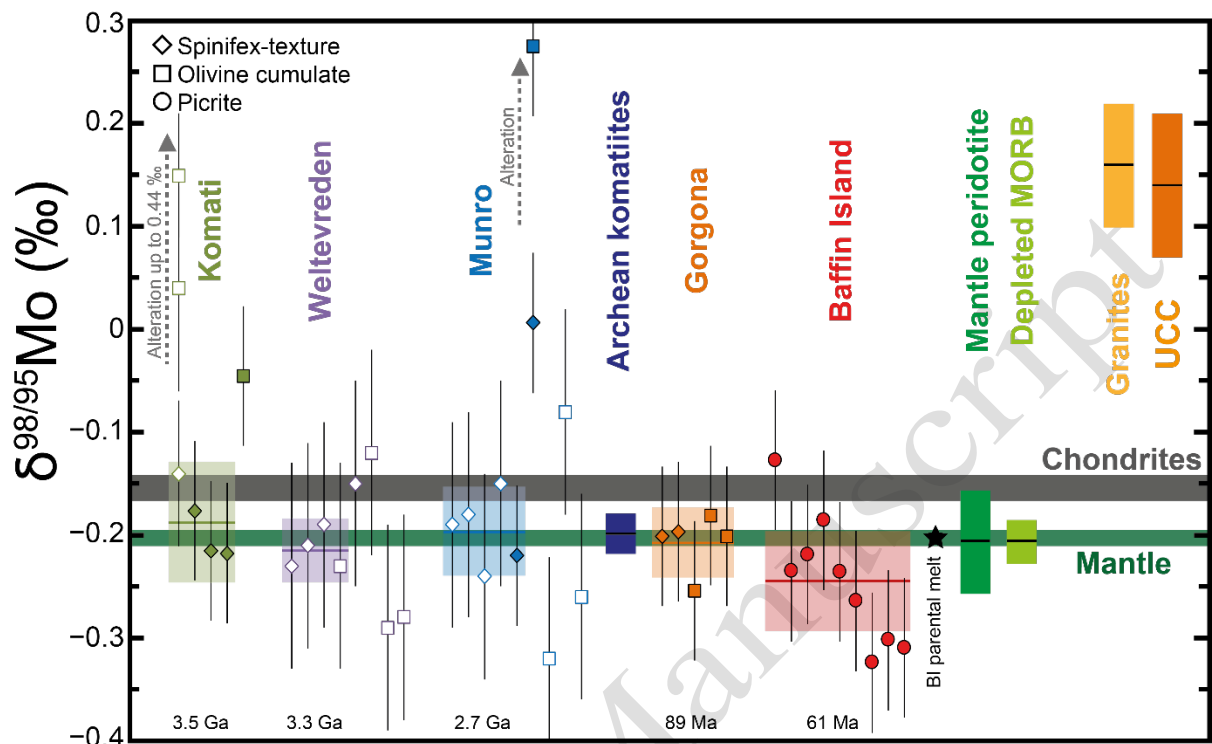


Figure 1: Variation of $\delta^{98}\text{Mo}$ in komatiites, picrites and major mantle and crustal reservoirs.

Filled symbols are data analysed herein with hollow symbols data taken from Greber et al. ¹⁷.

All individual analyses are plotted with the 2 standard deviation long term error, with the shaded areas for different formations and reservoirs the being 95% standard errors. The dark grey band represents chondritic meteorites ($\delta^{98}\text{Mo} = -0.154 \pm 0.013\text{‰}$; ^{11,12}) with the green bar representing the resolvable lighter depleted mantle ($\delta^{98}\text{Mo} = -0.204 \pm 0.008\text{‰}$; herein).

Average Archean komatiites ($\delta^{98}\text{Mo} = -0.199 \pm 0.019\text{‰}$; herein) with other reservoirs from ^{12,14,22} (see Table S3).

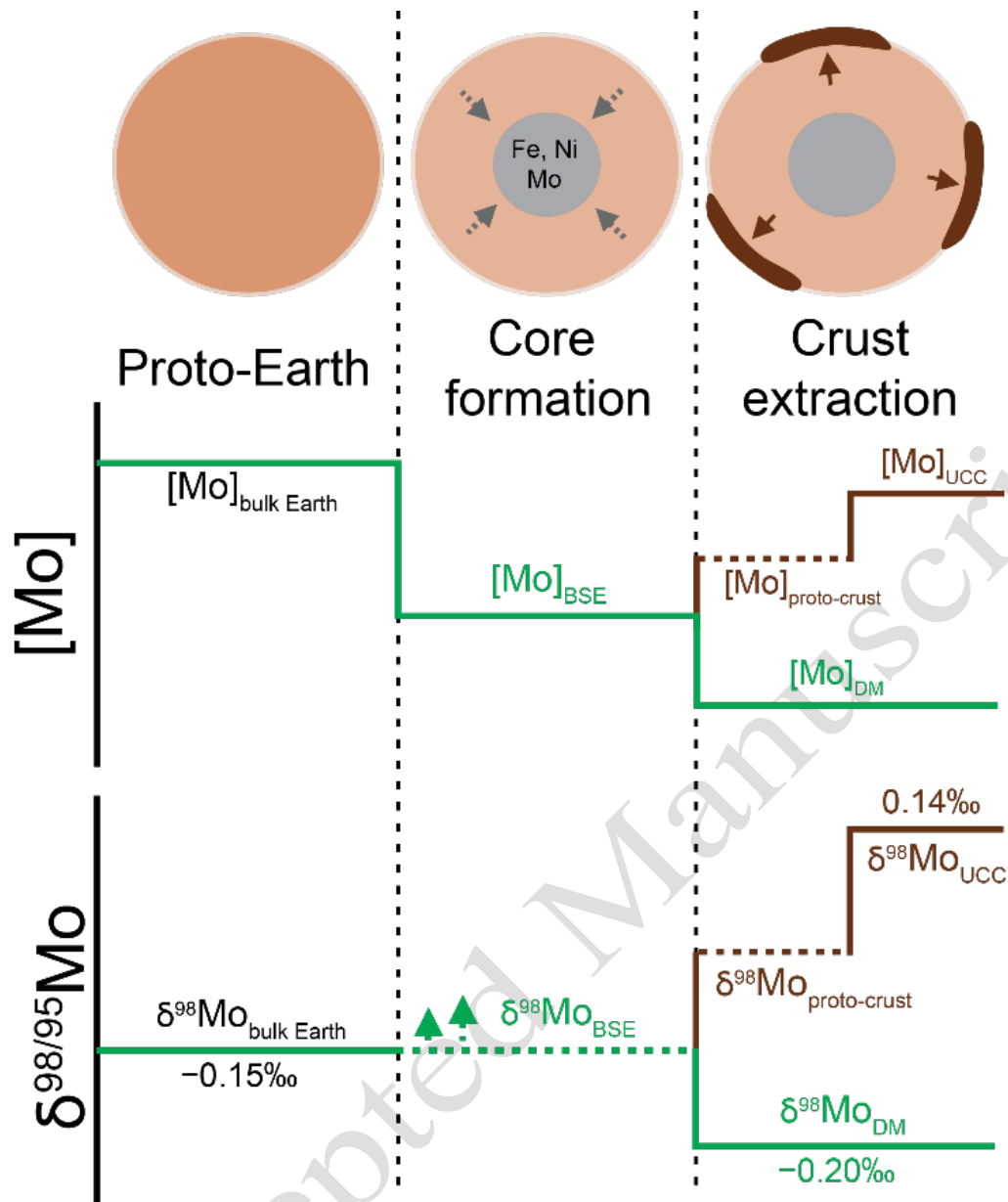


Figure 2: Schematic Mo evolution of Earth's mantle and crust during planetary differentiation. Earth accretes from chondritic meteorites thus the bulk Earth initial $\delta^{98}\text{Mo}$ will be chondritic. During core formation 95 % of Earth's Mo is sequestered into the core trapping isotopically light Mo in the metal phase, possibly making the residual BSE heavier. Subsequent extraction of Earth's isotopically heavy crust prior to 3.5 Ga resulted in a bulk mantle that is lighter than the building blocks of Earth. Earth's earliest crust was more mafic than modern crust and therefore had a different Mo concentration and isotopic composition.

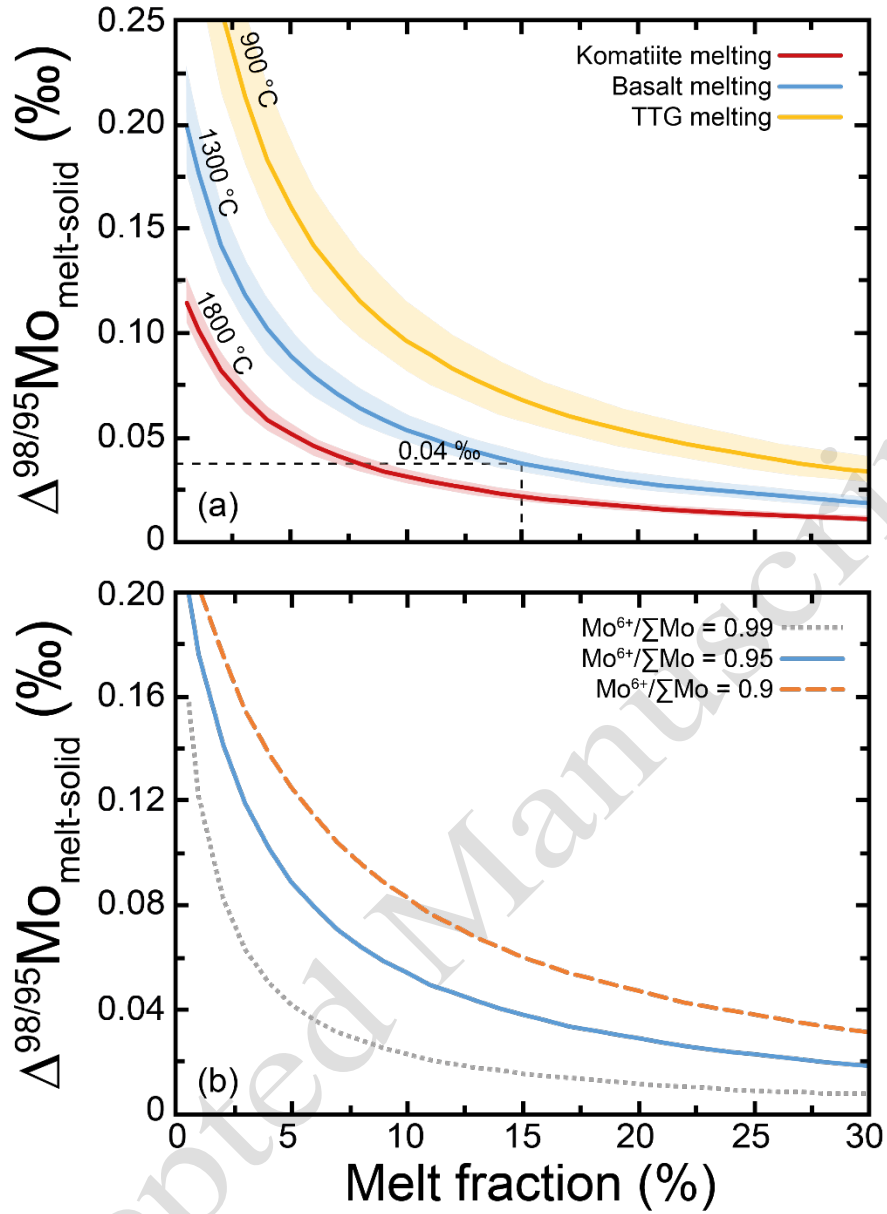


Figure 3: Partial melting model showing that the degree of enrichment of heavy Mo isotopes in the melt phase is controlled by both temperature and the valence state of Mo. (a) the effect of varying temperature at a constant oxygen fugacity ($\text{Mo}^{6+}/\Sigma\text{Mo} = 0.95$). Shaded areas represent varying the temperature by ± 100 °C. (b) The effect of varying oxygen fugacity at a constant temperature (1300 °C).

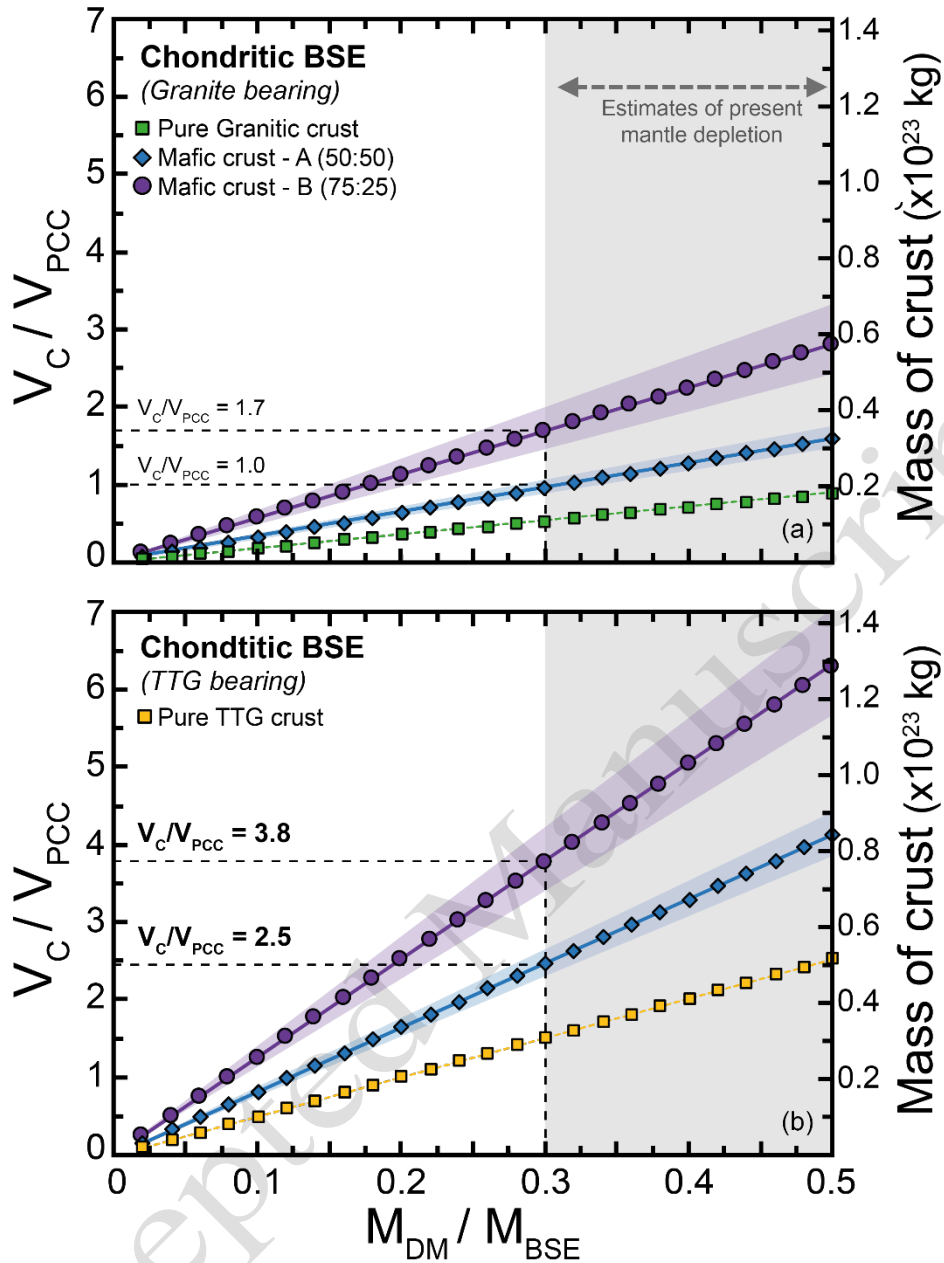


Figure 4: Results of Mo isotope mass balance calculations which estimate the mass of crust extraction required to balance the composition of the depleted mantle. This mass of crust can then be converted into a volume of crust (V_C) relative to the present volume of continental crust (V_{PCC}) and varies depending on the proportion of the total BSE that has undergone melt depletion (M_{DM}/M_{BSE}). Mafic crust-A and -B contain mafic and felsic rocks in 50:50 and 75:25 ratios, respectively. The shaded areas represent varying the proportions of the two endmembers by $\pm 5\%$.

Methods

Analytical Techniques

Molybdenum separation

All chemical separations were undertaken within the Arthur Holmes Isotope Geochemistry Laboratories at Durham University. The samples analysed herein have previously been extensively characterised^{23-26,51} with all powders created in Agate mills. Between 0.1-1.1 g of whole rock powder was weighed out to obtain ca. 30-150 ng of natural Mo and spiked with an equal amount of a ⁹⁷Mo–¹⁰⁰Mo double-spike to yield the ideal spike sample ratio of 1:1⁵². Two digestion methods were implemented in this study: 1) Most samples were digested in 15 mL Savillex beakers containing a 3:1 mixture of 29M HF + 16M HNO₃ on a hotplate at 130°C for ≥72 hours. Following evaporation, the samples were refluxed multiple times in 16M HNO₃, 12M HCl and 6M HCl to ensure complete decomposition of fluorides. For any samples that contained visible chromite or spinel grains the dissolved silicate portion was removed and saved, and an additional Parr bomb digestion step was undertaken to completely dissolve any refractory minerals. 2) Alternatively, carius tubes digestions were undertaken on some Baffin Island samples whereby ~1.0 g of sample powder was double spiked and mixed with 9 mL of reverse Aqua Regia (4:5 HCl-HNO₃), the tubes were subsequently sealed and heated to 220°C for >72 hours. Following cooling the carius tubes were opened and the supernatant and all undissolved silicate material was removed, using multiple rinses with MQ H₂O. This material was then further processed with a conventional HF-HNO₃ hotplate digestion, to dissolve the refractory silicate portion.

A leaching experiment was undertaken on two of the Baffin Island picrites (PI-37, PI-43; Table S5). A second aliquot of the same sample powder was sealed in a carius tube with 9 mL of reverse Aqua Regia (4:5 HCl-HNO₃) and heated to 220°C for >72 hours. Following

cooling the Aqua Regia supernatant was removed (henceforth the leachate; predominantly chromite and any sulfides present) and the remaining residual material (henceforth the residue; predominantly silicates) was then rinsed three times with MQ H₂O. The residue was then dried for reweighing and subsequently digested using conventional HF-HNO₃ digestion as described above. When fully dissolved the concentration of Mo in the two splits was obtained and the samples were spiked using the ⁹⁷Mo–¹⁰⁰Mo double spike and then refluxed several times in concentrated HNO₃ to equilibrate the spike and sample.

Chemical separation of Mo was achieved using anion exchange (AG1-x8) chromatography following the procedure described by Willbold, et al.⁵³. The samples are loaded onto the columns in 5 mL of 3M HCl + 0.05M ascorbic acid, the addition of ascorbic acid converts Fe³⁺ to Fe²⁺ which aids in elution of Fe from the anion exchange resin. This reaction is accompanied by a colour change from yellow to colourless when the reaction has been complete. Prior to loading all sample solutions were transferred into 15 mL centrifuge vials and centrifuged to remove any precipitates that may have formed in the dilute HCl loading solution. The sample matrix is then eluted in 3 mL of 3M HCl, 13 mL of 0.5M HCl + 0.5% H₂O₂, 10 mL of 1M HF and 3 mL of MQ H₂O, prior to collection of the purified Mo fraction in 12 mL of 1M HCl. Larger samples with >0.5g of material were loaded onto the columns in 10 mL of 3M HCl to ensure complete dissolution of the samples. These high mass samples were also processed through the complete chemical separation procedure twice to ensure the complete removal of Fe and Ru that can provide isobaric interferences during mass spectrometry. Total Mo procedural blanks calculated following double-spike deconvolution range from 0.18 to 0.30 ng (n = 7) and are considered negligible.

537 *Mass Spectrometry*

538 Molybdenum isotope compositions were measured using a Thermo-Finnigan Neptune multi-
 539 collector induction coupled plasma mass spectrometers (MC-ICP-MS). Samples were
 540 introduced using an Aridus II desolvating nebuliser and a low uptake rate Cetac35 nebuliser
 541 (aspiration rate 25-35 μLmin^{-1}). All measurements were made in low resolution using X-cones,
 542 and static collection mode with the simultaneous measurement of 9 isotopes ^{91}Zr , ^{92}Mo , ^{94}Mo ,
 543 ^{95}Mo , ^{96}Mo , ^{97}Mo , ^{98}Mo , ^{99}Ru and ^{100}Mo . Standard operation involved introduction of 150 ppb
 544 Mo double-spiked solutions in 0.5M HNO_3 and produced a maximum sensitivity of ~ 380
 545 Vppm^{-1} . Each analysis consisted of 1 block of 50 cycles with a 4 s integration time and was
 546 immediately preceded by the analysis of an acid blank, with a washout of 180 s occurring after
 547 each sample. Due to the low aspiration rate a single analysis used $<200 \mu\text{l}$ of solution. All Mo
 548 isotope measurements herein are reported relative to the internationally accepted reference
 549 solution the National Institute of Standards and Technology (NIST) SRM3134 ^{54,55} where
 550 $\delta^{98}\text{Mo} = 0\text{‰}$ as convention dictates. In all cases, conventional delta (δ) notation is used to
 551 express the ratios:

$$552 \quad \delta^{98/95}\text{Mo} = [((^{98}\text{Mo}/^{95}\text{Mo})_{\text{SAMPLE}}/(^{98}\text{Mo}/^{95}\text{Mo})_{\text{NIST 3134}}) - 1] \times 1000$$

553 Data reduction was carried out using the Isospike plugin ⁵⁶ for Iolite ⁵⁷ which is underpinned
 554 by the double spike deconvolution equations of Rudge, et al. ⁵². Baseline subtraction was
 555 undertaken using the 60 s of acid blank that immediately preceded a sample, with direct isobaric
 556 interferences from Zr on ^{92}Mo , ^{94}Mo and ^{96}Mo and Ru on ^{96}Mo , ^{98}Mo and ^{100}Mo mass
 557 fractionation corrected iteratively using the beta-factors calculated following the initial
 558 deconvolution. In addition to using the double spike to correct for instrumental mass
 559 fractionation, a secondary correction for within run mass spectrometer drift was applied using
 560 IsoSpike. The Mo isotope compositions of the unknowns were corrected using linear

interpolation by adjusting the composition of the bracketing analyses of the primary standard NIST3134, run at least every two unknowns, to 0‰.

The long-term stability of the mass spectrometer over a two-year period was confirmed by repeated measurement of the in-house standard Romil which has an average $\delta^{98}\text{Mo}$ of $0.045 \pm 0.027\text{‰}$ (2 s.d.; $n = 327$). Long-term accuracy was tested by repeated analyses of international standard solutions Open University ($-0.341 \pm 0.032\text{‰}$, $n = 58$) and Bern ($-0.242 \pm 0.029\text{‰}$, $n = 73$), which are within error of previous determinations^{40,55,58}. The reproducibility of analyses was further evaluated using a range of US Geological Survey rock standards. A range of first generation rock standards (BCR-1, BHVO-1, and AGV-1) were analysed here (see Table S1), multiple digestions ($n = 3-5$) reproduce to better than 0.031‰ , however, both BCR-1 and BHVO-1 have lower Mo concentrations and distinctly different $\delta^{98}\text{Mo}$ than their second generation counterparts (i.e. BHVO-2)^{11,59,60}, which suggests that these samples were contaminated with Mo during preparation of the second aliquot as suggested previously^{18,53}. Two separate digestions of low Mo (~ 30 ng/g) standard BIR-1 yield an average $\delta^{98}\text{Mo}$ of $-0.133 \pm 0.062\text{‰}$, which is within error of the previous estimate⁵³. Replicate digestions of the high mass, low Mo (30-75 ng/g) Baffin Island and komatiite samples herein generally reproduce to better than $\pm 0.10\text{‰}$, with two samples having significantly larger 2 s.d. (the statistics are poor with only two replicates) although their total range in $\delta^{98}\text{Mo}$ is $< 0.14\text{‰}$. Therefore, we conservatively consider $\pm 0.07\text{‰}$ as the long-term reproducibility of the measurements herein (the average 2 s.d. variability on the replicates herein is $\pm 0.068\text{‰}$; $n = 14$).

Mass balance calculations

The distribution of $\delta^{98}\text{Mo}$ between the depleted mantle and crust after differentiation can be estimated using isotopic and elemental mass balance (e.g. ¹⁸). For the present-day it is possible to calculate the mass of depleted mantle relative the total mantle using Nd isotopes because the mass of the present-day crust is well known, with previous studies suggesting that 30-50 % of whole mantle has been depleted ^{7,8,10,61}. Whereas for the early Earth these parameters remain poorly constrained and we need to make assumptions about crustal or mantle masses to undertake geochemical modelling. In this study, we measured Archean and Mesozoic primary magmas and found that have identical sub-chondritic Mo isotope compositions, therefore we conclude that the Paleoarchean mantle that produced the Barberton komatiites was equally depleted as the present-day mantle that produced the Gorgona komatiites. Since, present-day mantle depletion is the result of crust formation, it is logical to correlate that mantle depletion on the early Earth is also consequence of crust extraction. Given the range of present-day estimates of mantle depletion, by assuming at least 30 % mantle depletion had occurred by the Paleoarchean we can make inferences about the minimum volume of >3.5 Ga old crust that existed using mass modelling

The equations presented here are similar to those used previously ⁶². Here we consider that Mo of a portion of the *bulk silicate Earth* (BSE) has been accessed for crust formation and is distributed among two reservoirs; a *depleted mantle* (DM) and a *proto-crust* (C) (see Fig. S8). Given that at present-day that only 30-50 % of whole mantle has been depleted ^{7,8,10,61}, in the early Earth the mass of mantle sampled will be less than that of whole BSE, i.e. $m_{DM} < m_{BSE}$, and $m_{DM} = m_{BSE}$ only if the whole BSE mass has been used for crust extraction, which is probably not the case ^{7,8,10,61}.

The isotopic mass balance can be written as follows:

$$m_{BSE}[\text{Mo}]_{BSE} \delta_{BSE}^{98/95} = m_C[\text{Mo}]_C \delta_C^{98/95} + m_{DM}[\text{Mo}]_{DM} \delta_{DM}^{98/95} \quad (\text{A})$$

608 Where m is the mass, $[Mo]$ is the Mo concentration, and $\delta^{98/95}$ is the Mo isotope
 609 composition (i.e. $\delta^{98}Mo$) of the various reservoirs (BSE, DM and C).

610 The pure elemental mass balance is:

$$611 \quad m_{BSE}[Mo]_{BSE} = m_C[Mo]_C + m_{DM}[Mo]_{DM} \quad (B)$$

612 where, the terms denote similar meanings as above.

613 Substituting for “ $m_{AM}[Mo]_{BSE}$ ” in Eq. A by Eq. B, we have:

$$614 \quad m_C[Mo]_C \delta_C^{98/95} = (m_C[Mo]_C + m_{DM}[Mo]_{DM}) \delta_{BSE}^{98/95} - m_{DM}[Mo]_{DM} \delta_{DM}^{98/95}$$

$$615 \quad m_C[Mo]_C (\delta_C^{98/95} - \delta_{BSE}^{98/95}) = m_{DM}[Mo]_{DM} (\delta_{BSE}^{98/95} - \delta_{DM}^{98/95})$$

$$616 \quad m_C = \frac{m_{DM} \cdot [Mo]_{DM} \cdot (\delta_{BSE}^{98/95} - \delta_{DM}^{98/95})}{[Mo]_C \cdot (\delta_C^{98/95} - \delta_{BSE}^{98/95})} \quad (C)$$

617 This allows us to calculate the mass of crust generated assuming various amounts of
 618 depletion of the mantle reservoir (see Fig. 4).

619 The volume of this crust can then be calculated using the following:

$$620 \quad V_{crust} = m_{crust} / \rho_{crust} \quad (D)$$

621 where, V_c & ρ_c represent the volume and average density of the crust.

622 This volume is then easily comparable to the present volume of continental crust (PVCC)
 623 which is assumed to be $7.2 \times 10^9 \text{ km}^3$ ⁹. The parameters used in mass balance calculations herein
 624 are presented in Table S6. Here we have investigated two scenarios to encompass the
 625 variability of $\delta^{98}Mo$ and $[Mo]$ in Archean felsic rocks (granites or TTGs represent the felsic
 626 endmember; Fig. 4). Crustal volumes are then calculated for three different model Archean
 627 proto-crusts: a hypothetical purely felsic crust, Mafic crust-A (minimum based on a mafic
 628 crust) and Mafic crust-B (a likely Eoarchean crustal composition). The felsic crust is composed
 629 exclusively of granite or TTG rocks, while the Mafic crust-A and -B contain mafic rocks and
 630 felsic rocks in 50:50 and 75:25 proportions, respectively. Given the dominance of mafic

631 lithologies within the Earth's early crust >3 Ga^{45,46} it is reasonable to assume that the crust
632 extracted prior to 3.5 Ga was more mafic than today.

633

634 **Data Availability Statement**

635 All data generated during this study are included in the published article (and its
636 supplementary information files).

Accepted Manuscript

- 51 Kerr, A. C. La Isla de Gorgona, Colombia: A petrological enigma? *Lithos* **84**, 77-101,
doi:10.1016/j.lithos.2005.02.006 (2005).
- 52 Rudge, J. F., Reynolds, B. C. & Bourdon, B. The double spike toolbox. *Chemical Geology* **265**, 420-
431, doi:10.1016/j.chemgeo.2009.05.010 (2009).
- 53 Willbold, M. *et al.* High-Precision Mass-Dependent Molybdenum Isotope Variations in Magmatic
Rocks Determined by Double-Spike MC-ICP-MS. *Geostandards and Geoanalytical Research* **40**, 389-
403, doi:10.1111/j.1751-908X.2015.00388.x (2016).
- 54 Greber, N. D., Siebert, C., Nögler, T. F. & Petke, T. $^{898/95}\text{Mo}$ values and Molybdenum Concentration
Data for NIST SRM 610, 612 and 3134: Towards a Common Protocol for Reporting Mo Data.
Geostandards and Geoanalytical Research **36**, 291-300, doi:10.1111/j.1751-908X.2012.00160.x
(2012).
- 55 Goldberg, T. *et al.* Resolution of inter-laboratory discrepancies in Mo isotope data: An intercalibration.
Journal of Analytical Atomic Spectrometry **28**, 724-735, doi:10.1039/C3JA30375F (2013).
- 56 Creech, J. B. & Paul, B. IsoSpike: Improved Double-Spike Inversion Software. *Geostandards and
Geoanalytical Research* **39**, 7-15, doi:10.1111/j.1751-908X.2014.00276.x (2015).
- 57 Paton, C., Hellstrom, J., Paul, B., Woodhead, J. & Hergt, J. Iolite: Freeware for the visualisation and
processing of mass spectrometric data. *Journal of Analytical Atomic Spectrometry* **26**, 2508-2518
(2011).
- 58 Li, Y. *et al.* Controlling Mechanisms for Molybdenum Isotope Fractionation in Porphyry Deposits: The
Qulong Example. *Economic Geology* **114**, 981-992, doi:10.5382/econgeo.4653 (2019).
- 59 Zhao, P.-P. *et al.* Molybdenum Mass Fractions and Isotopic Compositions of International Geological
Reference Materials. *Geostandards and Geoanalytical Research* **40**, 217-226, doi:10.1111/j.1751-
908X.2015.00373.x (2015).
- 60 Yang, J. *et al.* Absence of molybdenum isotope fractionation during magmatic differentiation at Hekla
volcano, Iceland. *Geochimica et Cosmochimica Acta* **162**, 126-136, doi:10.1016/j.gca.2015.04.011
(2015).
- 61 Hofmann, A. W. Mantle geochemistry: the message from oceanic volcanism. *Nature* **385**, 219,
doi:10.1038/385219a0 (1997).
- 62 Jacobsen, S. B. & Wasserburg, G. J. The mean age of mantle and crustal reservoirs. *Journal of
Geophysical Research: Solid Earth* **84**, 7411-7427, doi:doi:10.1029/JB084iB13p07411 (1979).

Molybdenum isotope evidence for extensive crustal extraction in Earth's early history

Alex J. McCoy-West^{1, 2}, Priyadarshi Chowdhury², Kevin W. Burton¹, Paolo Sossi³, Geoff M. Nowell¹, J. Godfrey Fitton⁴, Andrew C. Kerr⁵, Peter A. Cawood² and Helen M. Williams^{1, 6}

¹Department of Earth Sciences, Durham University, Elvet Hill, Durham DH1 3LE, UK

²School of Earth, Atmosphere and Environment, Monash University, Clayton, Victoria, 3800, Australia

³Institute of Geochemistry and Petrology, ETH Zürich

⁴School of GeoSciences, University of Edinburgh, Edinburgh EH9 3FE, UK

⁵School of Earth and Ocean Sciences, Cardiff University, Park Place, Cardiff CF10 3AT, UK

⁶Department of Earth Sciences, University of Cambridge, Downing Street, Cambridge CB2 3EQ, UK

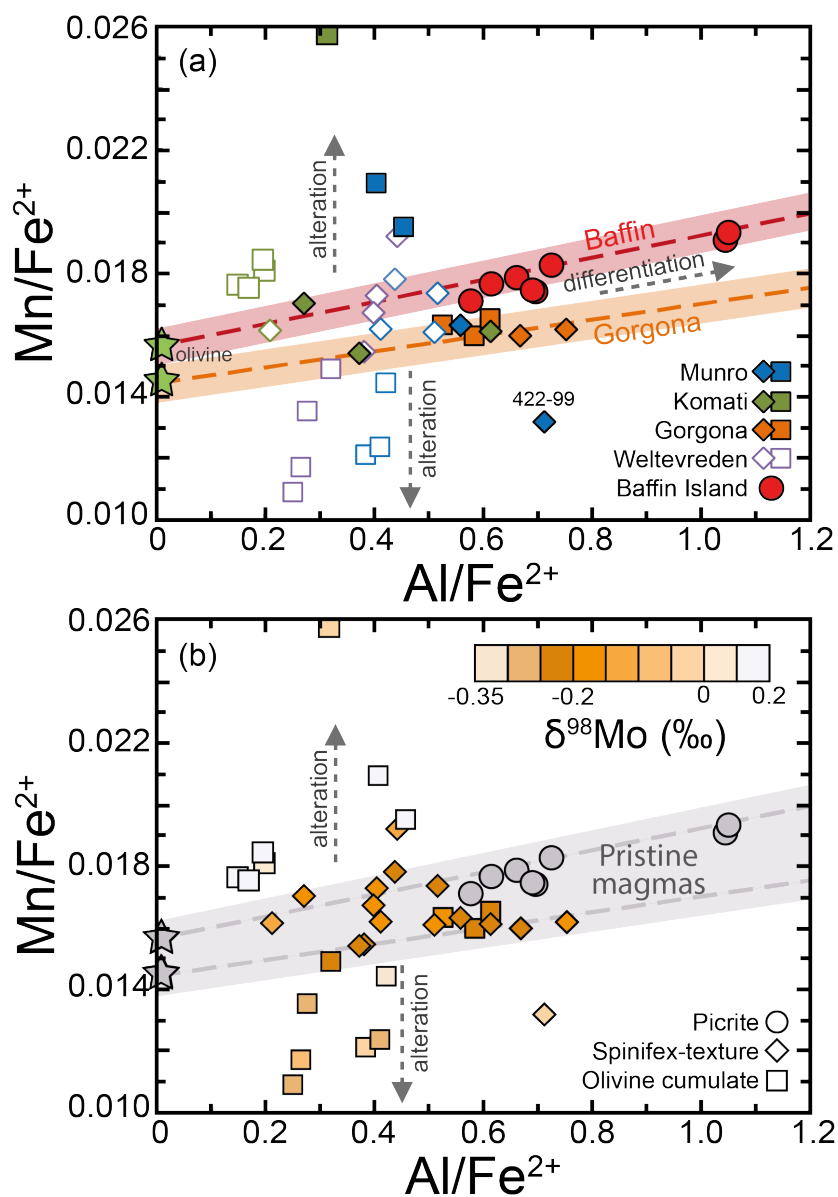
Corresponding author: Alex McCoy-West (alex.mccoywest@monash.edu)

Supplementary Figures 1-11

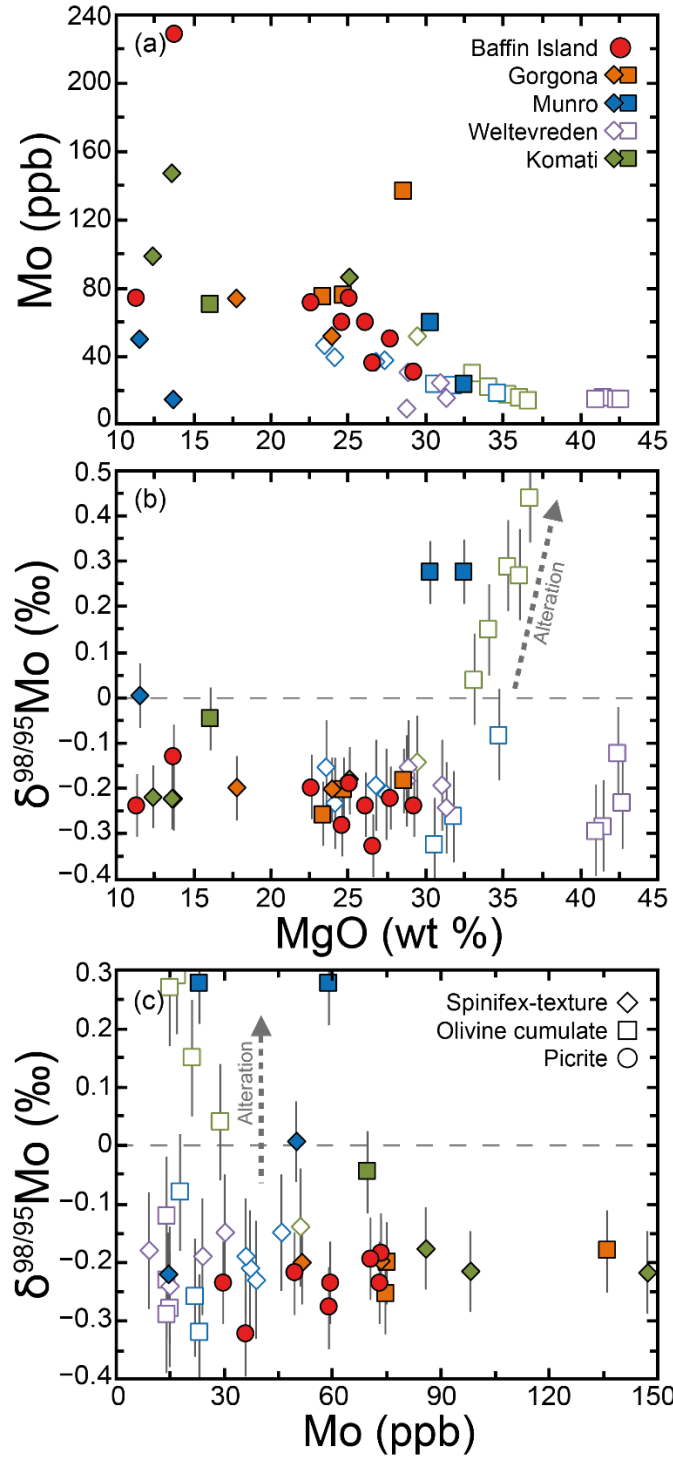
Supplementary Tables 1-10

Supplementary Text

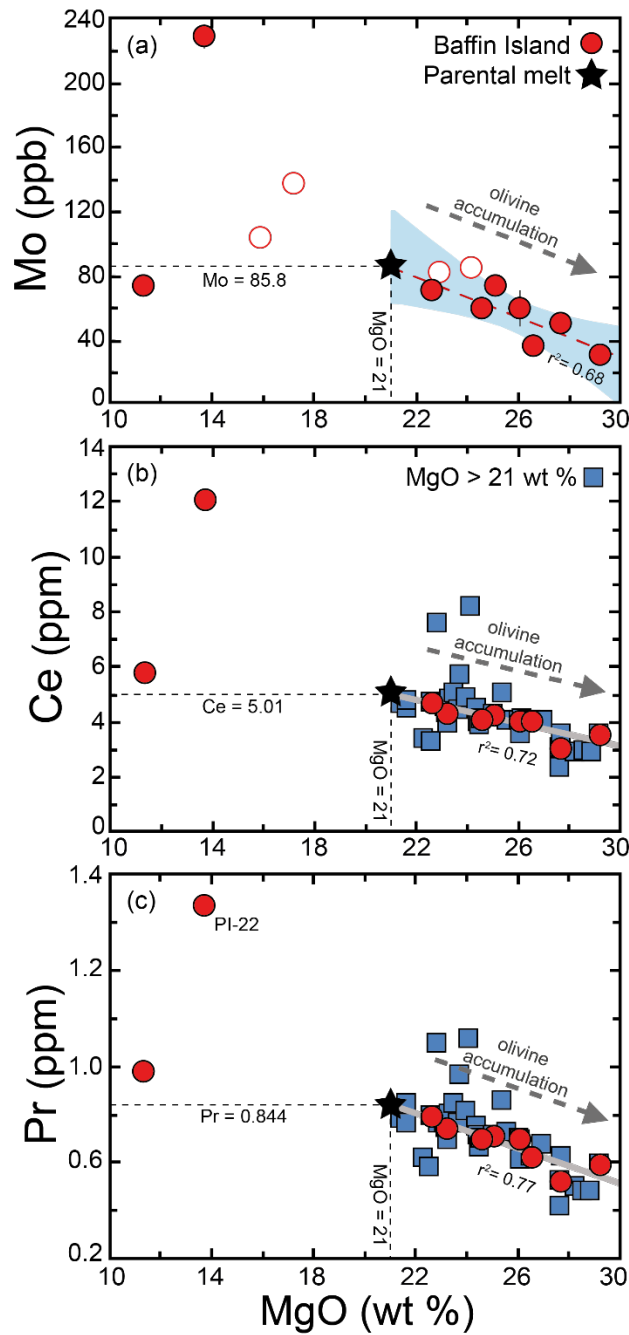
Figures and Tables



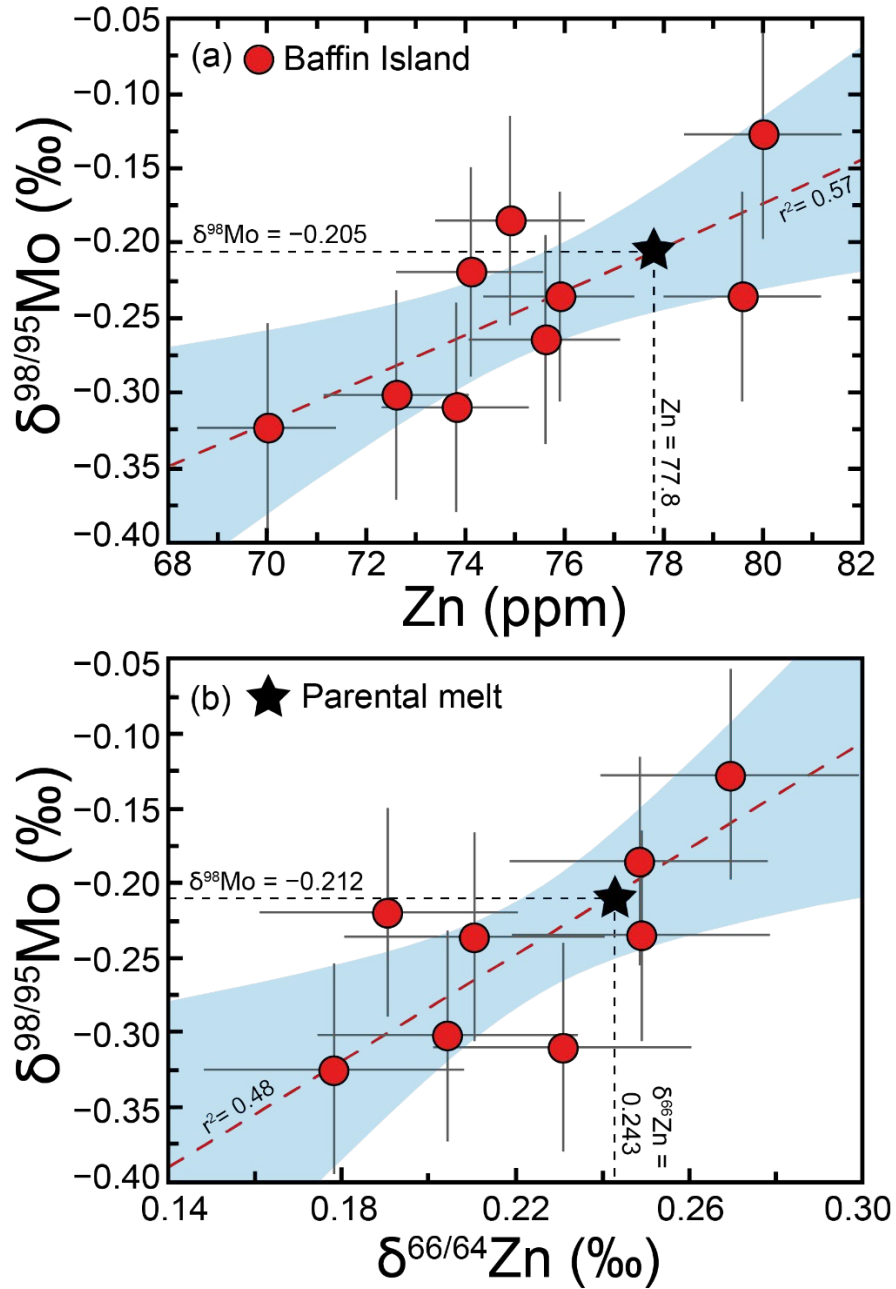
Supplementary Figure 1: Variation of Mn/Fe^{2+} versus Al/Fe^{2+} in komatiites and picrites. This type of plot is commonly used to assess alteration in komatiites^{1,2}. Different rock types are distinguished: picrites (circles), spinifex textured (diamonds) and olivine cumulates (squares). (a) Filled symbols represent samples analysed herein with hollow symbols samples measured in Greber, et al.³. Major element data comes from refs.⁴⁻⁸. The shaded red and orange fields represent pristine unaltered samples, based on Baffin Island picrites and Gorgona komatiites, with variations the result of accumulation or fractional crystallization of olivine crystals. Samples that fall perpendicular to this trend have experienced elemental mobility and are considered altered. (b) Komatiite data is coloured based on the $\delta^{98}\text{Mo}$ of the samples. Gradational scale uses 0.05‰ increments from and -0.35 to 0‰, and 0.1‰ increments above 0‰. All samples with $\delta^{98}\text{Mo} \geq 0.1\text{‰}$ are plotted with the light grey on the righthand side. Notably, samples with $\delta^{98}\text{Mo}$ between -0.25 and -0.15‰ plot near the unaltered field defined by the Baffin Island and Gorgona magmas.



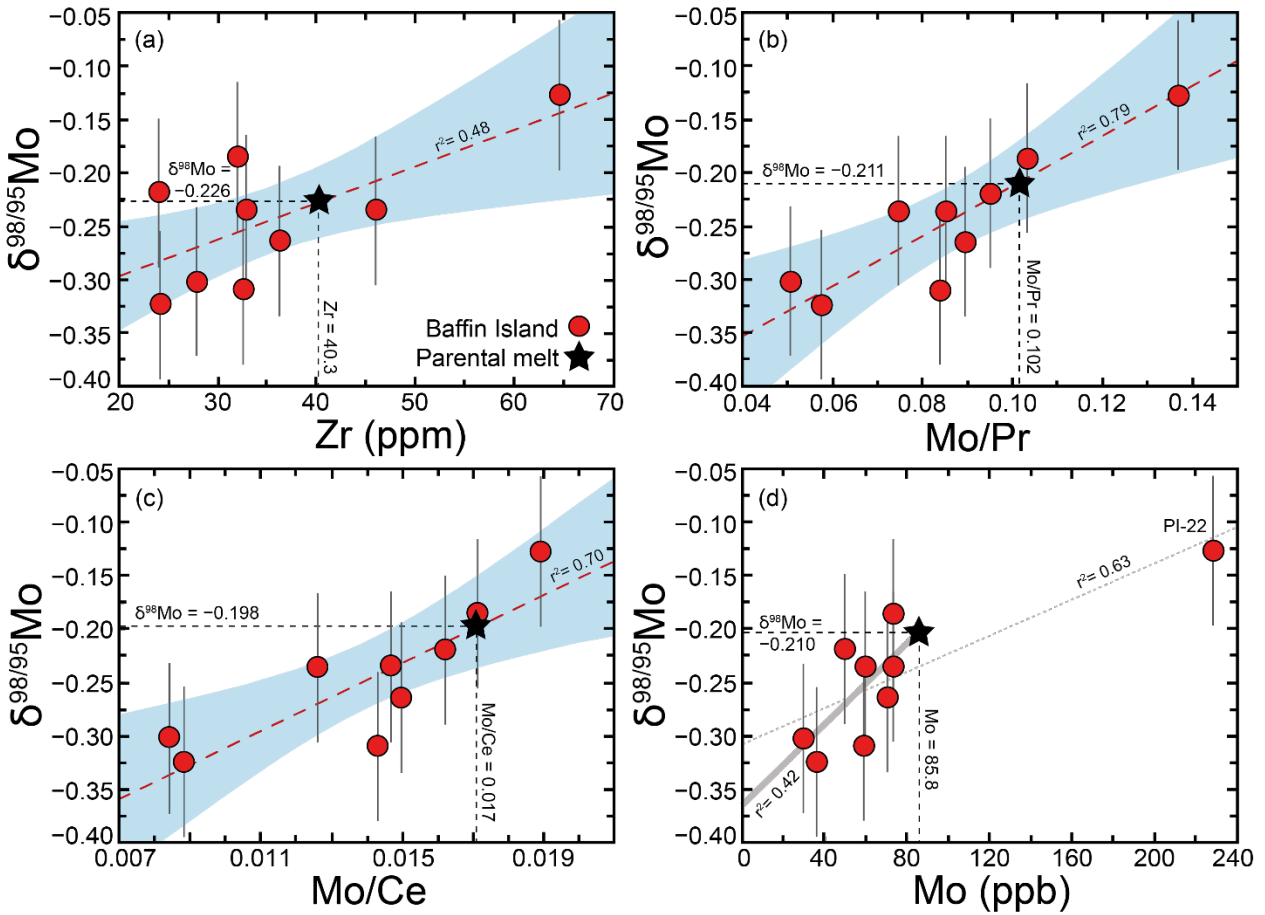
Supplementary Figure 2: Variation diagrams showing the MgO content, Mo concentration and $\delta^{98}\text{Mo}$ of komatiites and picrites. Filled symbols represent data analysed herein with hollow symbols samples investigated in Greber, et al. ³. Error bars on $\delta^{98}\text{Mo}$ are the average reproducibility of the Baffin Island analyses ($\pm 0.07\text{‰}$). No resolvable covariation is observed between $\delta^{98}\text{Mo}$ and MgO content. Notably, most spinifex texture lavas produce identical $\delta^{98}\text{Mo}$ within analytical errors at a wide range of Mo concentration, whereas the olivine cumulates have invariable Mo concentrations but more variation in $\delta^{98}\text{Mo}$ due to their greater proportion of olivine which is susceptible to alteration.



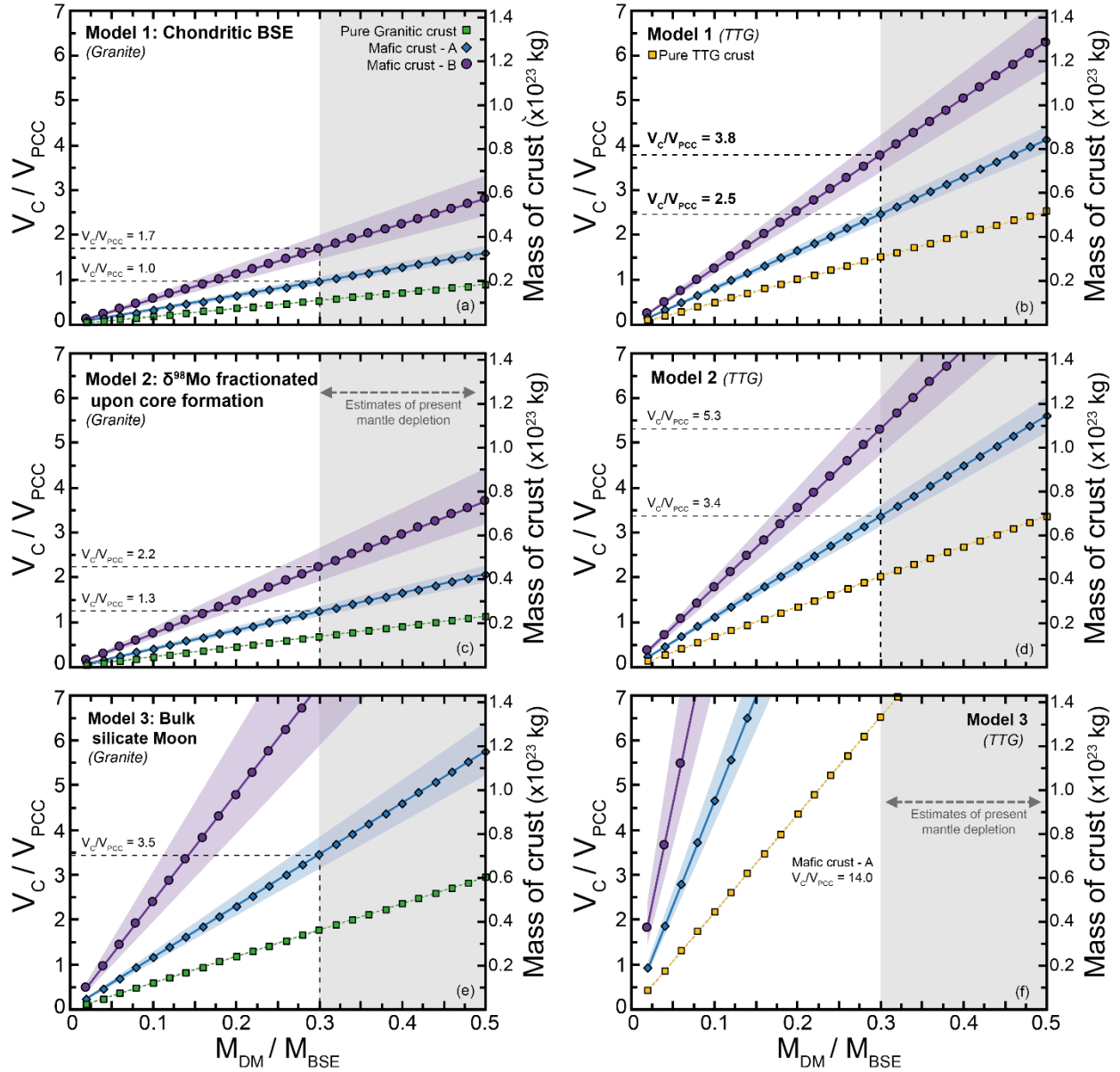
Supplementary Figure 3: Trace element evidence for olivine accumulation in high-MgO Baffin Island picrites. Excellent correlations are observed against MgO in samples with >21 wt % MgO. (a) Variation of Mo concentration versus MgO content. Hollow symbols are samples with only concentration data. Shaded area represents the 95% confidence interval of the correlation. (b-c) Ce and Pr concentration, respectively, versus MgO content. Whole rock data comes from Starkey, et al. ⁶ with the complete Baffin Island dataset (squares) plotted for comparison. The parental melt (i.e. the original composition of the magmas from the mantle source region corrected for olivine accumulation) at Baffin Island was calculated to have 21 wt % MgO (see McCoy-West, et al. ⁹ for detailed discussion).



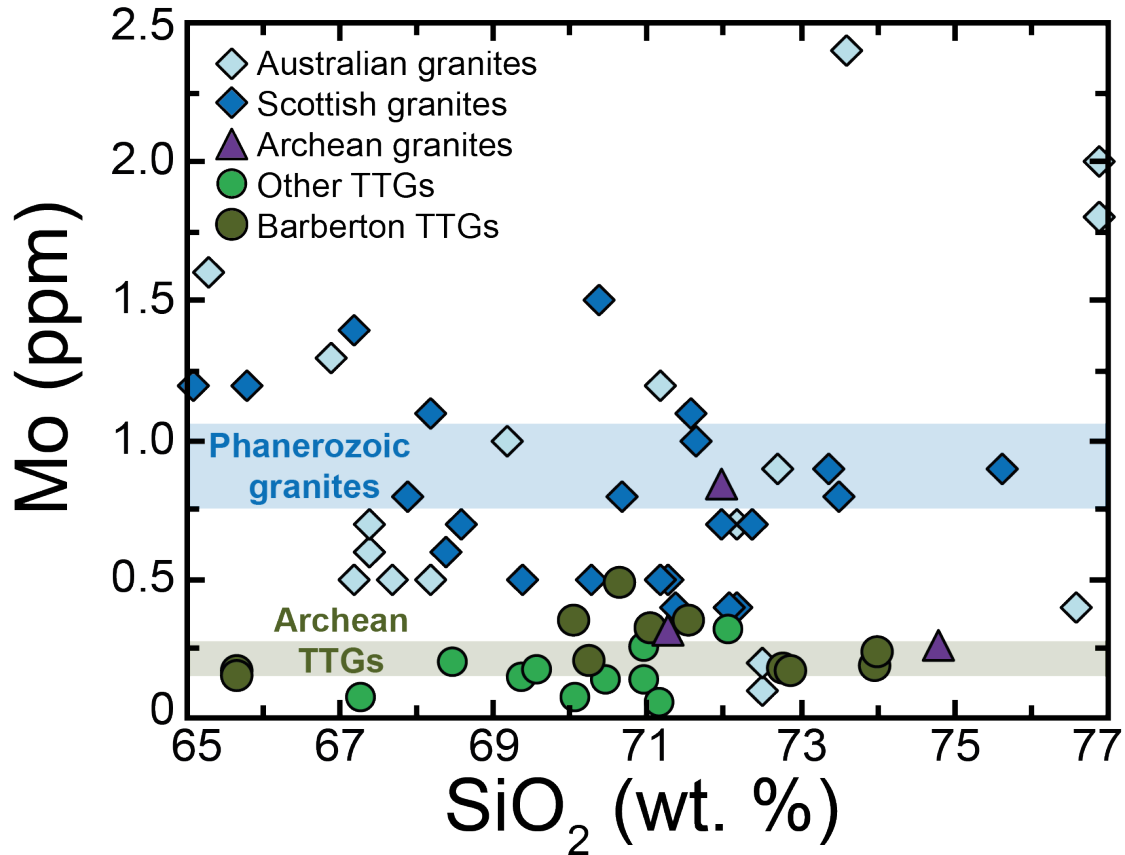
Supplementary Figure 4: Variation diagrams of $\delta^{98}\text{Mo}$ versus Zn concentration (a) and $\delta^{66}\text{Zn}$ (b). Comparative Zn data come from Starkey, et al. ⁶ and McCoy-West, et al. ⁹. Shaded area represents the 95% confidence interval of the correlation. Error bars on $\delta^{98}\text{Mo}$ are the average reproducibility of the Baffin Island analyses ($\pm 0.07\text{‰}$), with errors on Zn concentration assumed to be 2% and $\delta^{66}\text{Zn}$ the long-term reproducibility ($\pm 0.03\text{‰}$). The correlation between Zn concentration and $\delta^{66}\text{Zn}$ and the Mo isotope compositions suggests that the variability is controlled by the same process (i.e. olivine accumulation). See McCoy-West, et al. ⁹ for more detailed discussion of the accumulation of olivine phenocrysts that have experienced kinetic isotope exchange based on Fe and Zn isotopes.



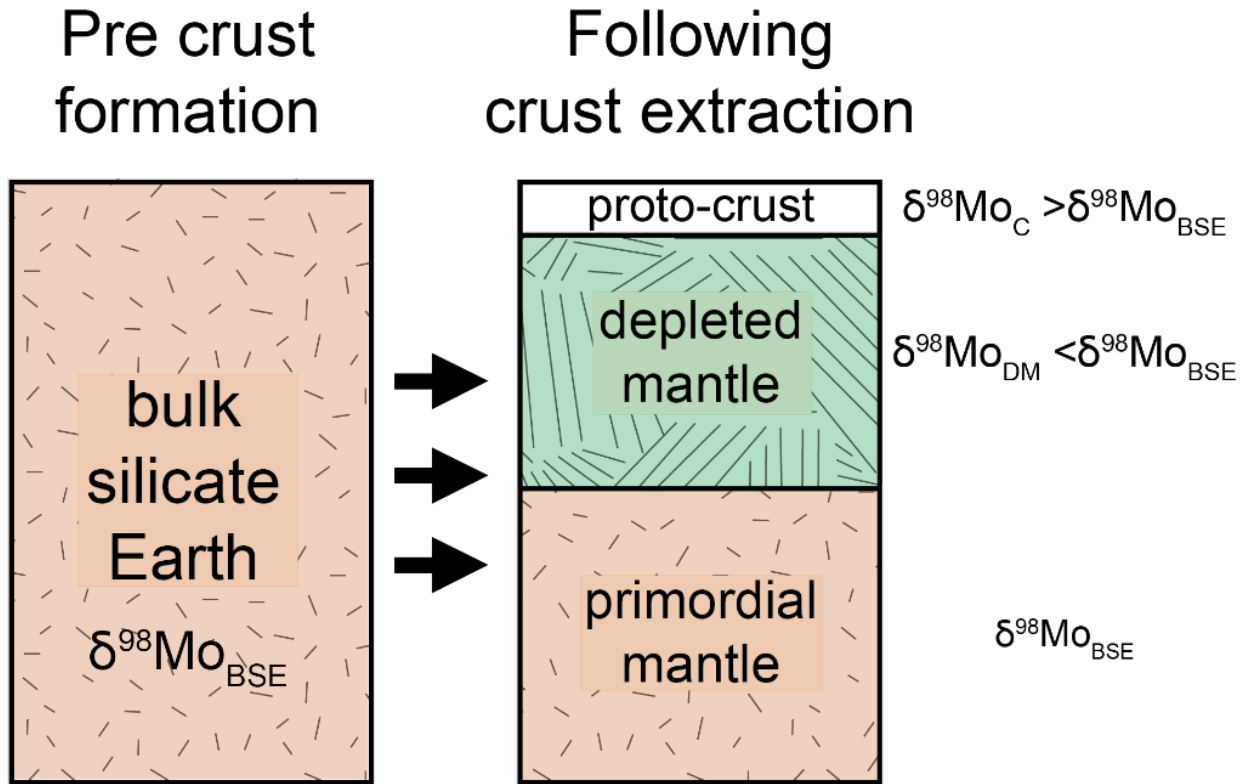
Supplementary Figure 5: Variation diagrams of $\delta^{98}\text{Mo}$ versus trace element concentrations or elemental ratios in the Baffin Island picrites. Comparative data come from Starkey, et al. ⁶. Shaded areas represent the 95% confidence interval on the correlations. Error bars on $\delta^{98}\text{Mo}$ are the average reproducibility of the analyses ($\pm 0.07\text{‰}$). The strong correlations between MgO content and trace elements (see Fig. S3) allow calculation of the elemental concentration of the parental melt (i.e. 21 wt % MgO). This value is then used with the correlations presented above to obtain the $\delta^{98}\text{Mo}$ of the parental melt (see Table S2). The strong linear trends show this is the result of accumulation (i.e. a linear addition process) rather than magmatic differentiation (where parabolic curves would be expected).



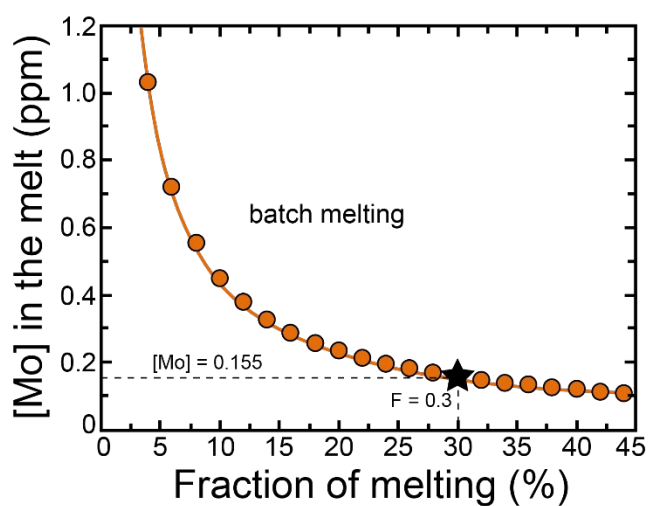
Supplementary Figure 6: Results of Mo isotope mass balance calculations which estimate the mass of crust extraction required to balance the composition of the depleted mantle. This mass of crust can then be converted into a volume of crust (V_C) relative to the present volume of continental crust (V_{PCC}) and varies depending on the proportion of the total BSE that has undergone melt depletion (M_{DM}/M_{BSE}). Thirty to fifty percent depletion of the mantle (grey field) can reproduce the radiogenic isotope and incompatible element signatures of the crust and depleted mantle, assuming they represent complementary reservoirs¹⁰⁻¹³. (a-b) Model 1: assumes a chondritic BSE for Mo isotopes ($\delta^{98}\text{Mo} = -0.154\%$; as shown in the main text); (c-d) Model 2: assumes an isotopically heavier BSE following core formation ($\delta^{98}\text{Mo} = -0.142\%$). (e) Model 3: assumes the BSE equilibrated with the composition of the silicate Moon ($\delta^{98}\text{Mo} = -0.078\%$). Crustal volumes are calculated for three different Archean crust types: a purely felsic crust, Mafic crust-A (minimum based on a mafic crust) and Mafic crust-B (a likely Archean crustal composition). Felsic-crust is composed exclusively of felsic rocks, while the Mafic crust-A and -B contain mafic and felsic rocks in 50:50 and 75:25 ratios, respectively. The felsic endmember is either granite (left side: a, c, e) or more realistic for the early Earth has a TTG composition (b, d, f; see Table S6 for further details).



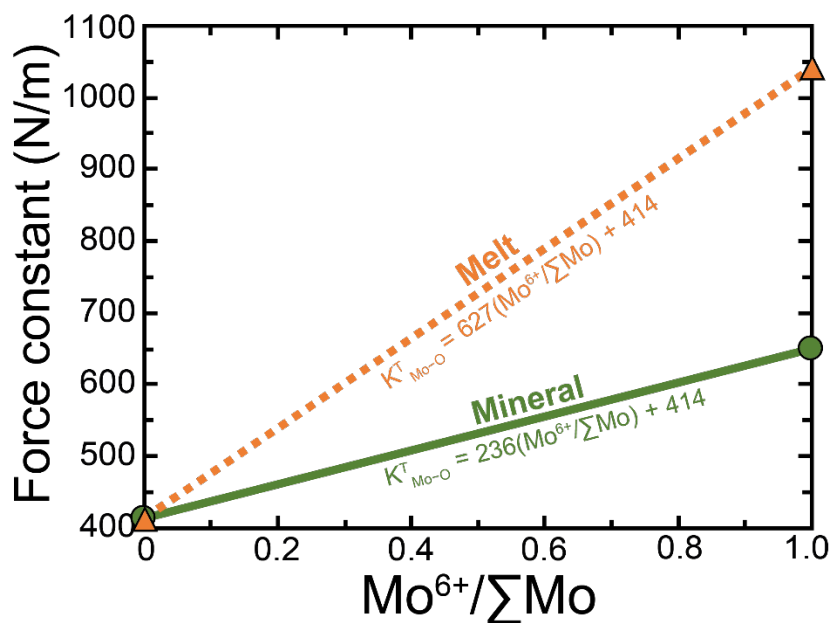
Supplementary Figure 7: Comparison of the Mo concentration of Phanerozoic granites and Archean granites and tonalite-trondhjemite-granodiorites (TTGs). Archean samples come from Greaney, et al. ¹⁴ and are divided into Barberton TTGs (3.2-3.6 Ga), other TTGs (Zimbabwe and Superior; 2.7-3.0 Ga) and granites (2.6-2.7 Ga). Phanerozoic samples come from Yang, et al. ¹⁵, they are divided on the basis of location into Australian (Lachlan and New England orogens; 286-428 Ma) and Scottish (Caledonian plutons; 392-408 Ma) samples. Shaded bars represent the averages for Archean TTGs (Mo = 0.21 ± 0.05 ppm; n = 26; ¹⁴) and Phanerozoic granites (Mo = 0.90 ± 0.15 ppm; n = 46; ¹⁵).



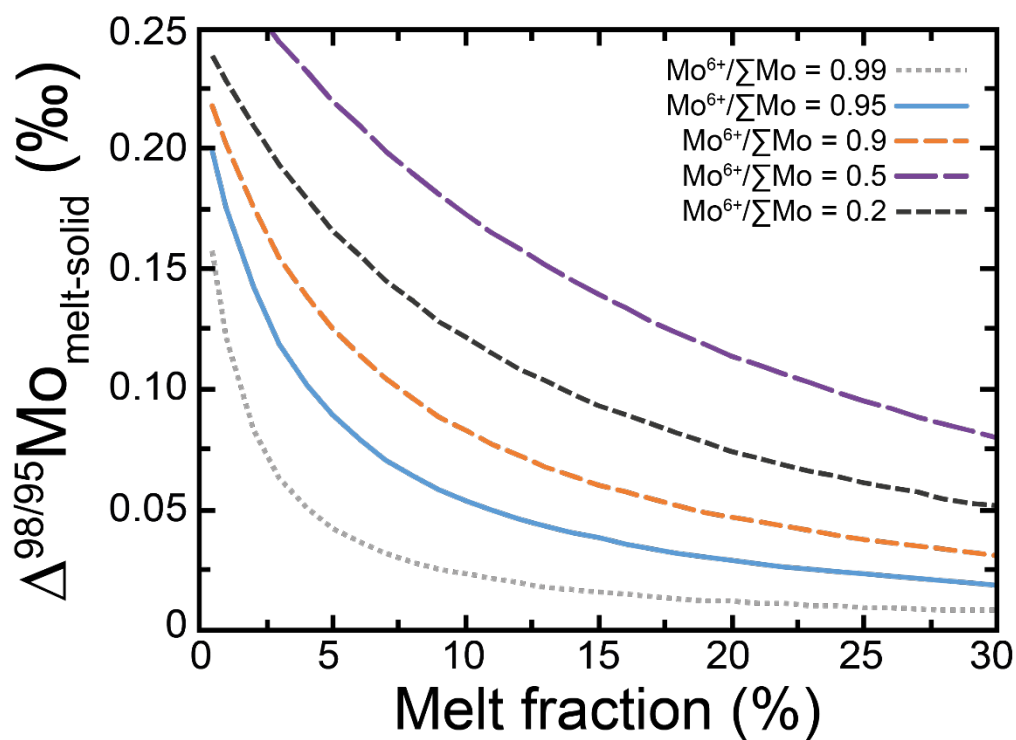
Supplementary Figure 8: During crust formation a portion of the bulk silicate Earth (BSE) is tapped and distributed among two reservoirs; a depleted mantle (DM) and a proto-crust (C). Given that only 30-50 % of whole mantle has been depleted to form the crust: $m_{\text{DM}} + m_{\text{C}} \ll m_{\text{BSE}}$, meaning a primordial mantle reservoir remains untapped.



Supplementary Figure 9: Batch melting model showing the variation in Mo concentration as a function of melt fraction. Modelling uses a bulk D_{Mo} of 0.006¹⁶ and assumes a source concentration of 0.047 ppm¹⁷. The [Mo] of the basalt endmember (0.155) is based on 30% melting of the mantle (sitting in the middle of the Archean range to produce a high Mg basalt; ^{18,19}).



Supplementary Figure 10: Force constant of Mo–O bonds in minerals and melt as a function of $\text{Mo}^{6+}/\Sigma\text{Mo}$ used in the modelling presented in Figure 4 and Tables S9 and S10. Based on values presented in Table S8.



Supplementary Figure 11: Partial melting model showing that the degree of enrichment of heavy Mo isotopes in the melt phase as a function of oxygen fugacity ($\text{Mo}^{6+}/\Sigma\text{Mo}$) at a constant temperature (1300 °C). Highly reduced conditions do not reflect the conditions on the modern Earth but are relevant to melting on celestial bodies (e.g. Moon, Angrites). Tabulated values can be found in Table S10.

Supplementary Table 1: Molybdenum concentrations and isotope compositions of high-degree partial melts and reference materials.

| Sample | Location | Rock Type | MgO (wt%) | Mo (ng/g) | | | $\delta^{98/95}\text{Mo}$ | | | n |
|--------------------------------------|--------------------|-----------|-----------|-----------|-------|-------------|---------------------------|---------|---------------|---|
| | | | | a | b | Average | a | b | Average | |
| <u>Baffin Island</u> | | | | | | | | | | |
| PI-22 | Padloping Island | pic | 13.7 | 226.0 | 231.4 | 229 ±7.6 | -0.092 | -0.162 | -0.127 ±0.098 | 2 |
| PI-24 | | pic | 26.1 | 55.6 | 63.5 | 59.6 ±11.2 | -0.243 | -0.227 | -0.235 ±0.023 | 2 |
| PI-25 | | pic | 27.7 | 49.6 | 49.3 | 49.4 ±0.4 | -0.181 | -0.257* | -0.219 ±0.107 | 2 |
| PI-26 | | pic | 25.1 | 74.0 | 72.7 | 73.3 ±1.8 | -0.169 | -0.202* | -0.186 ±0.047 | 2 |
| PI-28 | Durban Island | pic | 11.3 | 75.4 | 73.0 | 73.0 ±3.4 | -0.244 | -0.227* | -0.236 ±0.024 | 2 |
| PI-31~ | | pic | 22.6 | 69.8 | 71.3 | 70.5 ±2.2 | -0.333 | -0.195 | -0.264 ±0.195 | 2 |
| PI-37 | | pic | 26.6 | 35.9 | 35.6 | 35.8 ±0.4 | -0.305 | -0.343* | -0.324 ±0.054 | 2 |
| PI-40~ | | pic | 29.2 | 30.0 | 29.6 | 29.8 ±0.6 | -0.235 | -0.369* | -0.302 ±0.189 | 2 |
| PI-43 | | pic | 24.6 | 58.5 | 59.0 | 58.8 ±0.6 | -0.342 | -0.278* | -0.310 ±0.090 | 2 |
| PAD-6^ | | pic | 17.6 | 137.1 | - | | | | | |
| DI-23^ | | pic | 24.1 | 84.8 | - | | | | | |
| DI-26^ | | pic | 15.9 | 102.9 | - | | | | | |
| DUR-8^ | | pic | 22.9 | 82.1 | - | | | | | |
| <u>Gorgona</u> | | | | | | | | | | |
| GOR94-29 | Gorgona Island | STK | 17.8 | 73.3 | | | -0.197 | - | -0.197 ±0.070 | 2 |
| GOR94-43 | | STK | 23.9 | 49.6 | 53.1 | 51.4 ±4.9 | -0.213 | -0.189 | -0.201 ±0.034 | |
| GOR94-3 | | OC | 28.6 | 135.8 | | | -0.181 | - | -0.181 ±0.070 | |
| GOR94-17 | | OC | 23.4 | 74.6 | | | -0.254 | - | -0.254 ±0.070 | |
| GOR94-44 | | OC | 24.7 | 75.2 | | | -0.201 | - | -0.201 ±0.070 | |
| <u>Lower Komati</u> | | | | | | | | | | |
| 331/777a | Komati | STK | 25.1 | 85.7 | 87.8 | 86.7 ±3.0 | -0.169 | -0.184 | -0.177 ±0.021 | 2 |
| 331/778 | | STB | 12.3 | 98.3 | - | | -0.216 | - | -0.216 ±0.070 | |
| 331/786 | | STB | 13.6 | 147.1 | - | | -0.218 | - | -0.218 ±0.070 | |
| 331/790# | Mundt's Concession | OC | 16.1 | 69.6 | 60.3 | 64.9 ± 13.1 | -0.070 | -0.020 | -0.045 ±0.070 | 2 |
| <u>Munro</u> | | | | | | | | | | |
| 422/84# | Pyke Hill | OC | 30.3 | 59.1 | - | | 0.276 | - | 0.276 ±0.070 | 2 |
| 422/86# | | OC | 32.4 | 23.1 | - | | 0.277 | - | 0.277 ±0.070 | |
| 422/99# | Red Lake | STB | 11.5 | 49.9 | - | | 0.007 | - | 0.007 ±0.070 | |
| RL-12-1 | | STB | 13.7 | 14.4 | 22.2 | 18.2 ±10.7 | -0.242 | -0.198 | -0.220 ±0.062 | |
| <u>Mid-ocean ridge basalt</u> | | | | | | | | | | |
| 45N | Mid-Atlantic | E-type | | 403 | 418 | 410 ±21 | -0.198 | -0.119 | -0.159 ±0.056 | 2 |
| <u>Rock Standards</u> | | | | | | | | | | |
| AGV-1 | Oregon | and | 1.5 | 2186 | 2062 | 2101 | -0.154 | -0.168 | | 3 |
| | | | | 2055 | | ±147 | -0.169 | | -0.164 ±0.017 | |
| BCR-1 | Oregon | bas | 3.5 | 1741 | 1676 | 1682 | 0.066 | 0.076 | | 3 |
| | | | | 1630 | | ±111 | 0.079 | | 0.074 ±0.013 | |
| BIR-1 | Iceland | bas | 9.7 | 32.2 | 34.1 | 33.1 ±2.6 | -0.111 | -0.155 | -0.133 ±0.062 | 2 |
| BHVO-1 | Hawaii | bas | 7.2 | 1077 | 1092 | | -0.219 | -0.220 | | 5 |
| | | | | 1025 | 1103 | 1061 | -0.205 | -0.182 | | |
| | | | | 1006 | | ±85 | -0.200 | | -0.205 ±0.031 | |

Errors on average Mo concentrations and $\delta^{98/95}\text{Mo}$ are two-standard deviations. For samples with only one replicate the average reproducibility of the Baffin Island samples is taken as the error (± 0.07 ‰; see the methods section for further discussion). Sample types: pic = picrite; OC = olivine cumulate; STK = spinifex texture komatiite; STB = spinifex texture basalt; bas = basalt; and = andesite. # samples are altered and not included in calculating the average composition of Archean komatiites. * denotes samples that were digested initially using carius tube digestion then followed by HF-HNO₃ digestion. ^ samples that were only run initially for concentrations by isotope dilution. ~ Two samples did not reproduce very well and the 2 s.d. are large, however, the total range between the replicates is significantly smaller.

Supplementary Table 2: Calculation of the Mo isotope composition of the Baffin Island parental melt.

| Parameter | Regressions | Value at 21 wt % MgO | $\delta^{98/95}\text{Mo}$ (‰) |
|-------------------------------|--------------------------|----------------------|--------------------------------------|
| Zn (ppm) | Fig. S3 ($r^2 = 0.57$) | 77.8 | -0.205 ± 0.040 |
| $\delta^{66}\text{Zn}$ (‰) | Fig. S3 ($r^2 = 0.48$) | 0.243 | -0.212 ± 0.050 |
| Mo/Pr | Fig. S4 ($r^2 = 0.79$) | 0.102 | -0.211 ± 0.043 |
| Mo/Ce | Fig. S4 ($r^2 = 0.70$) | 0.017 | -0.198 ± 0.043 |
| Zr (ppm) | Fig. S4 ($r^2 = 0.48$) | 40.3 | -0.226 ± 0.035 |
| Mo (ppb) | Fig. S4 ($r^2 = 0.42$) | 85.8 | -0.210 ± 0.068 |
| Average Parental Melt: | | | -0.210 ± 0.010 |

Errors on $\delta^{98}\text{Mo}$ are calculated from the 95 % confidence interval (error envelopes) on the regressions calculated using Isoplot ²⁰ at the composition of the parental melt. The MgO content of the Baffin Island parental melt was calculated at 21 wt. % MgO using the inflection method (see McCoy-West, et al. ⁹). Given the strong correlations between elemental concentration and MgO content in the picrites with >21 wt. % MgO, using linear regression concentrations of the elements of interest are calculated at the parental melt composition. Zn isotope data comes from McCoy-West, et al. ⁹. Trace earth element data is from Starkey, et al. ⁶.

Supplementary Table 3: Locations and Mo isotope compositions of primitive materials used to calculate the Mo isotope composition of the accessible mantle.

| Location | $\delta^{98/95}\text{Mo}$ (‰) | 2 s.d. | n | References |
|------------------------------|--------------------------------------|-------------------------------|---|--------------------------------------|
| <i>Depleted-MORB</i> | | | | |
| Pacific-Antarctic Ridge | -0.206 ± 0.021 | ± 0.033 | 5 | Bezard, et al. ²¹ |
| <i>Phanerozoic picrite</i> | | | | |
| Baffin Island, NE Canada | -0.210 ± 0.10 | ± 0.019 | 6 | Herein |
| <i>Phanerozoic komatiite</i> | | | | |
| Gorgona, Columbia | -0.207 ± 0.034 | ± 0.055 | 5 | Herein |
| <i>Archean komatiites</i> | | | | |
| Komati, South Africa | -0.187 ± 0.059 | ± 0.074 | 4 | Herein; Greber, et al. ³ |
| Weltevreden, South Africa | -0.215 ± 0.038 | ± 0.031 | 4 | Greber, et al. ³ |
| Munro, Canada | -0.196 ± 0.044 | ± 0.070 | 5 | Greber, et al. ³ ; Herein |
| <i>Mantle Xenoliths</i> | | | | |
| Tariat, Mongolia | -0.210 ± 0.093 | ± 0.177 | 6 | Liang, et al. ²² |
| Vitim, Siberia | -0.198 ± 0.061 | ± 0.077 | 4 | Liang, et al. ²² |
| Accessible Mantle | -0.204 ± 0.008 | ± 0.018 | 8 | Herein |

Errors on $\delta^{98}\text{Mo}$ are 95% standard errors (95% s.e. = $t * \text{s.d.}/(n)^{1/2}$, where t = inverse survival function of the Student's t-test at the 95% significance level and (n-1) degrees of freedom), with two-standard deviation (2 s.d.) also shown to represent population uncertainty. Depleted mid ocean ridge basalts (MORB) are only those samples with measured $^{143}\text{Nd}/^{144}\text{Nd} \geq 0.513117$. Mantle xenoliths from Kilbourne Hole, New Mexico were excluded due to their large spread in $\delta^{98}\text{Mo}$ values (0.32 ‰) and limited sample set (n = 3).

Supplementary Table 4: Molybdenum isotope compositions of geochemical reservoirs presented in Figure 1 or used in modelling.

| Reservoir | $\delta^{98/95}\text{Mo}$ (‰) | 2 s.d. | <i>n</i> | References |
|-------------------------|-------------------------------|-------------|----------|---------------------------------------------------------------|
| Chondrites | -0.154 ± 0.013 | ± 0.051 | 18 | Liang, et al. ²² , Burkhardt, et al. ²³ |
| Archean komatiites | -0.199 ± 0.019 | ± 0.062 | 13 | Herein |
| Mantle peridotites | -0.206 ± 0.050 | ± 0.180 | 15 | Liang, et al. ²² |
| Global basalts | -0.10 ± 0.04 | ± 0.27 | 57 | Yang, et al. ¹⁵ and therein |
| Global granites | 0.16 ± 0.05 | ± 0.41 | 55 | Yang, et al. ¹⁵ and therein |
| Upper Continental Crust | 0.14 ± 0.07 | | 112 | Yang, et al. ¹⁵ |

Errors on $\delta^{98}\text{Mo}$ are 95% standard errors (95% s.e. = $t * \text{s.d.}/(n)^{1/2}$, where t = inverse survival function of the Student's t -test at the 95% significance level and $(n-1)$ degrees of freedom), with two-standard deviation (2 s.d.) also shown to represent population uncertainty. Chondrite average excludes CK and CM groups meteorites, like in ²³. Upper continental crust composition was calculated assuming a 10:1 proportion of felsic to basaltic rocks ¹⁵.

Supplementary Table 5: Leaching experiments on Baffin Island picrites.

| Sample | Whole Rock | | Residue (Silicates) | | Leachate (Non-silicates) | |
|--------|------------|---------------------------|---------------------|---------------------------|--------------------------|---------------------------|
| | Mo (ng/g) | $\delta^{98/95}\text{Mo}$ | Mo (ng) | $\delta^{98/95}\text{Mo}$ | Mo (ng) | $\delta^{98/95}\text{Mo}$ |
| PI-37 | 35.8 | -0.324 ± 0.054 | ~11 | -0.323 ± 0.054 | ~7 | -0.403 ± 0.051 |
| PI-43 | 58.8 | -0.310 ± 0.090 | ~16 | -0.263 ± 0.026 | ~10 | -0.374 ± 0.034 |

A second aliquot of the same sample powder was sealed in a carius tube with 9 mL of reverse aqua regia (4:5 HCl-HNO₃) and heated to 220°C for >72 hours. Following cooling the aqua regia supernatant was removed (henceforth the leachate; predominantly chromite and any sulfides present) and the remaining residual material (henceforth the residue; predominantly silicates) were spiked and processed separately through chemistry.

Supplementary Table 6: Molybdenum concentration and isotopes compositions of geochemical reservoirs used in mass balance calculations.

| Reservoir | Mass (kg) ^a | Density (kg/m ³) | Mo (ppm) | $\delta^{98/95}\text{Mo}$ (‰) |
|-------------------------------|---------------------------|---------------------------------|------------------------------|----------------------------------|
| Chondrites | | | ca. 1.7 ^b | $-0.154 \pm 0.013^{\text{f,g}}$ |
| Earth | 5.9376×10^{24} | | | |
| Core | 1.932×10^{24} | | ca. 5 ^b | $-0.16 \pm 0.02^{\text{f}}$ |
| Bulk silicate Earth | 4.0603×10^{24} | | $0.047 \pm 0.019^{\text{c}}$ | -0.154 |
| Mantle | 4.0343×10^{24} | | | |
| Depleted mantle | Varied | | $0.025 \pm 0.007^{\text{d}}$ | -0.204 ± 0.008 |
| Modern crust | 2.6×10^{22} | | | |
| Mafic endmember | | 3000 | 0.155 | $-0.10 \pm 0.04^{\text{h}}$ |
| Types of Crust | | | | |
| <i>Granite bearing models</i> | | | | |
| Pure Granitic crust | | 2750 | 0.47 ^d | $0.16 \pm 0.07^{\text{h}}$ |
| Mafic crust A (50:50) | | 2850 ± 15 | 0.313 ± 0.016 | 0.096 ± 0.010 |
| Mafic crust B (75:25) | | 2925 ± 15 | 0.234 ± 0.016 | 0.031 ± 0.018 |
| <i>TTG bearing models</i> | | | | |
| Pure TTG crust | | 2750 | 0.28 ^d | 0.03 |
| Mafic crust A (50:50) | | 2850 ± 15 | 0.218 ± 0.006 | -0.016 ± 0.006 |
| Mafic crust B (75:25) | | 2925 ± 15 | 0.186 ± 0.006 | -0.051 ± 0.008 |

Mafic crust compositions were calculated by mixing different proportions of mafic and felsic material (i.e. 75:25 is 75% mafic). Molybdenum concentration data shows that Phanerozoic granites are clearly more evolved than their Archean counterparts (see Fig. S7). The Mo concentration of the felsic endmembers were taken from the available published data in Greaney, et al. ¹⁴, using the average composition of the oldest 3.5 Ga Barberton TTGs (0.28; n = 15), and 2.7 Ga granites (0.47; n = 3) available. The Mo concentration of the mafic endmember (Mo = 0.155) was calculated based on batch melting of the bulk silicate Earth assuming an F of 0.3 (higher than today due to the elevated mantle temperatures in the Eoarchean) and a bulk D_{Mo} of 0.006 ¹⁶ (see Fig. S9). The isotopic composition of mafic endmember uses the modern global basalt average of $\delta^{98}\text{Mo} = -0.10 \pm 0.04$ ‰ (n = 57). Partial melting is a time invariant process at constant temperature and therefore the modern basalts provide a good analogue. The formation of TTGs requires the remelting of metabasalt, given that TTGs have lower Mo concentrations than granites it is sensible to assume their $\delta^{98}\text{Mo}$ will also be less evolved. Here we have taken the simplest approach (i.e. two step formation of TTGs) and taken the average of global basalts and granites to estimate the $\delta^{98}\text{Mo}$ of TTG felsic component. Densities were calculated by mixing basaltic (3000 kg/m³) and granitic (2700 kg/m³) endmembers. Errors on Mafic crusts (A and B) represent varying the proportions of the two endmembers by 5%. References for other parameters as follows: a) Yoder ²⁴; b) McDonough ²⁵; c) Palme and O'Neill ¹⁷; d) Salters and Stracke ²⁶; e) Rudnick and Gao ²⁷; f) Burkhardt, et al. ²³; g) Liang, et al. ²²; h) Yang, et al. ¹⁵.

Supplementary Table 7: Model parameters for the calculation of Mo isotope fractionation during non-modal batch melting.

| Phase | Starting fraction* | Melting reaction* | D_{Mo4+}^{\wedge} | D_{Mo6+}^{\wedge} |
|---------------|--------------------|-------------------|---------------------|---------------------|
| Olivine | 0.6 | -0.15 | 0.5 | 0.006 |
| Orthopyroxene | 0.25 | 0.15 | 0.7 | 0.009 |
| Clinopyroxene | 0.1 | 1.0 | 0.3 | 0.001 |

*Melting parameters come from Walter ²⁸. [^] Partition coefficients are taken from Leitzke, et al. ²⁹. Model assumes that the force constant is a linear function of $Mo^{6+}/\sum Mo$ for both minerals and melt and that all minerals have the same $Mo^{6+}/\sum Mo$. Modelling uses force constants calculated in Table S8.

Supplementary Table 8: Parameters used for the calculation of force constants of Mo isotopes in minerals and melts at varied oxidation state.

| | \overline{Z}_{Mo} | $C_{N_{Mo}}$ | \overline{S}_{Mo} | \overline{S}_O | r_{Mo-O}^M (Å) | r_{Mo-O}^{Cal} (Å) | $K_{f_{Mo-O}}$ (N/m) | K_{Mo-O}^T (N/m) |
|--------------------------|---------------------|--------------|---------------------|------------------|---------------------|-------------------------|-------------------------|-----------------------|
| <u>Melt</u> | | | | | | | | |
| $Mo^{6+}O_4(2-)$ | 6 | 4 | 1.5 | 0.5 | 1.76 ¹ | 1.79 | 349.8 | 1040.8 |
| <u>Minerals</u> | | | | | | | | |
| $Mo^{6+}O_3$ | 6 | 6 | 1.0 | 0.67 | 1.98 ² | 1.98 | 218.4 | 649.8 |
| <u>Minerals and Melt</u> | | | | | | | | |
| $Mo^{4+}O_2$ | 4 | 6 | 0.67 | 0.67 | 2.01 ³ | 2.03 | 139.2 | 414.1 |

\overline{Z}_{Mo} = cation charge; $C_{N_{Mo}}$ = coordination number. \overline{S}_{Mo} and \overline{S}_O is the average bond valence of molybdenum and oxygen, respectively. r_{Mo-O}^M = measured Mo–O bond length. Measured Mo–O bond lengths are from 1) Farges et al. ³⁰; 2) Kihlborg ³¹; 3) Brandt and Skapski ³². r_{Mo-O}^{Cal} = calculated Mo–O bond length are based on the approximation that the mean Mo–O bond distance is the sum of the Shannon ionic radius for these species in the appropriate coordination environment and that of O^{2-} (1.38 Å). $K_{f_{Mo-O}}$ = is the force constant approximated by solving the Born-Landé equation. K_{Mo-O}^T = is the total force constant corrected by a scaling factor related to the proportion of ionic bonds (the ionicity of the Mo–O bond based on the Pauling scale is 0.336). The mean coordination number of oxygen was reported as 3 minerals ^{31,32}, with a coordination number of 4 for oxygen reported for Mo^{6+} melt complexes ³⁰. All formulas required for calculating force constants can be found in Sossi and O'Neill ³³.

Supplementary Table 9: Results of partial melting modelling showing the change $\Delta^{98}\text{Mo}_{\text{melt-solid}}$ as a function of temperature ($^{\circ}\text{C}$) at a constant oxygen fugacity ($\text{Mo}^{6+}/\Sigma\text{Mo} = 0.95$) as shown in Figure 3.

| Temp | 800 | 900 | 1000 | 1200 | 1300 | 1400 | 1700 | 1800 | 1900 |
|-------|-------|-------|-------|-------|-------|-------|-------|-------|-------|
| F | | | | | | | | | |
| 0.005 | 0.429 | 0.359 | 0.305 | 0.228 | 0.200 | 0.177 | 0.127 | 0.115 | 0.105 |
| 0.01 | 0.378 | 0.317 | 0.269 | 0.201 | 0.176 | 0.156 | 0.112 | 0.101 | 0.092 |
| 0.02 | 0.305 | 0.256 | 0.217 | 0.162 | 0.142 | 0.126 | 0.090 | 0.082 | 0.074 |
| 0.03 | 0.255 | 0.214 | 0.181 | 0.136 | 0.119 | 0.105 | 0.076 | 0.069 | 0.062 |
| 0.04 | 0.219 | 0.183 | 0.156 | 0.116 | 0.102 | 0.090 | 0.065 | 0.059 | 0.053 |
| 0.05 | 0.192 | 0.160 | 0.136 | 0.102 | 0.089 | 0.079 | 0.057 | 0.051 | 0.047 |
| 0.06 | 0.170 | 0.142 | 0.121 | 0.090 | 0.079 | 0.070 | 0.050 | 0.046 | 0.041 |
| 0.07 | 0.152 | 0.128 | 0.108 | 0.081 | 0.071 | 0.063 | 0.045 | 0.041 | 0.037 |
| 0.08 | 0.138 | 0.116 | 0.098 | 0.073 | 0.064 | 0.057 | 0.041 | 0.037 | 0.034 |
| 0.09 | 0.126 | 0.105 | 0.089 | 0.067 | 0.059 | 0.052 | 0.037 | 0.034 | 0.031 |
| 0.10 | 0.116 | 0.097 | 0.082 | 0.061 | 0.054 | 0.048 | 0.034 | 0.031 | 0.028 |
| 0.11 | 0.107 | 0.089 | 0.076 | 0.057 | 0.050 | 0.044 | 0.032 | 0.029 | 0.026 |
| 0.12 | 0.099 | 0.083 | 0.070 | 0.053 | 0.046 | 0.041 | 0.029 | 0.027 | 0.024 |
| 0.13 | 0.092 | 0.077 | 0.066 | 0.049 | 0.043 | 0.038 | 0.027 | 0.025 | 0.023 |
| 0.14 | 0.087 | 0.072 | 0.061 | 0.046 | 0.040 | 0.036 | 0.026 | 0.023 | 0.021 |
| 0.15 | 0.081 | 0.068 | 0.058 | 0.043 | 0.038 | 0.033 | 0.024 | 0.022 | 0.020 |
| 0.16 | 0.077 | 0.064 | 0.054 | 0.041 | 0.036 | 0.031 | 0.023 | 0.021 | 0.019 |
| 0.17 | 0.072 | 0.061 | 0.051 | 0.038 | 0.034 | 0.030 | 0.021 | 0.019 | 0.018 |
| 0.18 | 0.068 | 0.057 | 0.049 | 0.036 | 0.032 | 0.028 | 0.020 | 0.018 | 0.017 |
| 0.19 | 0.065 | 0.054 | 0.046 | 0.034 | 0.030 | 0.027 | 0.019 | 0.017 | 0.016 |
| 0.20 | 0.062 | 0.052 | 0.044 | 0.033 | 0.029 | 0.025 | 0.018 | 0.017 | 0.015 |
| 0.21 | 0.059 | 0.049 | 0.042 | 0.031 | 0.027 | 0.024 | 0.017 | 0.016 | 0.014 |
| 0.22 | 0.056 | 0.047 | 0.040 | 0.030 | 0.026 | 0.023 | 0.017 | 0.015 | 0.014 |
| 0.23 | 0.053 | 0.045 | 0.038 | 0.028 | 0.025 | 0.022 | 0.016 | 0.014 | 0.013 |
| 0.24 | 0.051 | 0.043 | 0.036 | 0.027 | 0.024 | 0.021 | 0.015 | 0.014 | 0.012 |
| 0.25 | 0.049 | 0.041 | 0.035 | 0.026 | 0.023 | 0.020 | 0.014 | 0.013 | 0.012 |
| 0.26 | 0.047 | 0.039 | 0.033 | 0.025 | 0.022 | 0.019 | 0.014 | 0.013 | 0.011 |
| 0.27 | 0.045 | 0.038 | 0.032 | 0.024 | 0.021 | 0.019 | 0.013 | 0.012 | 0.011 |
| 0.28 | 0.043 | 0.036 | 0.031 | 0.023 | 0.020 | 0.018 | 0.013 | 0.012 | 0.011 |
| 0.29 | 0.042 | 0.035 | 0.030 | 0.022 | 0.019 | 0.017 | 0.012 | 0.011 | 0.010 |
| 0.30 | 0.040 | 0.034 | 0.029 | 0.021 | 0.019 | 0.017 | 0.012 | 0.011 | 0.010 |

Supplementary Table 10: Results of partial melting modelling showing the change $\Delta^{98}\text{Mo}_{\text{melt-solid}}$ as a function oxygen fugacity ($\text{Mo}^{6+}/\Sigma\text{Mo}$) as at a constant oxygen temperature (1300 °C) as shown in Figure S10.

| $\text{Mo}^{6+}/\Sigma\text{Mo}$ | 0.99 | 0.95 | 0.90 | 0.50 | 0.20 | 0.01 |
|----------------------------------|-------|-------|-------|-------|-------|-------|
| F | | | | | | |
| 0.005 | 0.158 | 0.200 | 0.218 | 0.279 | 0.238 | 0.207 |
| 0.01 | 0.122 | 0.176 | 0.202 | 0.271 | 0.228 | 0.160 |
| 0.02 | 0.083 | 0.142 | 0.176 | 0.256 | 0.209 | 0.109 |
| 0.03 | 0.063 | 0.119 | 0.155 | 0.243 | 0.193 | 0.082 |
| 0.04 | 0.051 | 0.102 | 0.138 | 0.230 | 0.179 | 0.066 |
| 0.05 | 0.042 | 0.089 | 0.125 | 0.219 | 0.166 | 0.054 |
| 0.06 | 0.036 | 0.079 | 0.114 | 0.208 | 0.155 | 0.046 |
| 0.07 | 0.032 | 0.071 | 0.104 | 0.198 | 0.145 | 0.040 |
| 0.08 | 0.028 | 0.064 | 0.096 | 0.189 | 0.136 | 0.035 |
| 0.09 | 0.025 | 0.059 | 0.089 | 0.180 | 0.128 | 0.031 |
| 0.10 | 0.023 | 0.054 | 0.083 | 0.172 | 0.121 | 0.028 |
| 0.11 | 0.021 | 0.050 | 0.077 | 0.164 | 0.115 | 0.026 |
| 0.12 | 0.019 | 0.046 | 0.072 | 0.157 | 0.109 | 0.023 |
| 0.13 | 0.018 | 0.043 | 0.068 | 0.150 | 0.103 | 0.021 |
| 0.14 | 0.017 | 0.040 | 0.064 | 0.144 | 0.098 | 0.020 |
| 0.15 | 0.015 | 0.038 | 0.060 | 0.138 | 0.093 | 0.018 |
| 0.16 | 0.014 | 0.036 | 0.057 | 0.133 | 0.089 | 0.017 |
| 0.17 | 0.014 | 0.034 | 0.054 | 0.128 | 0.085 | 0.016 |
| 0.18 | 0.013 | 0.032 | 0.052 | 0.123 | 0.081 | 0.015 |
| 0.19 | 0.012 | 0.030 | 0.049 | 0.118 | 0.078 | 0.014 |
| 0.20 | 0.012 | 0.029 | 0.047 | 0.114 | 0.075 | 0.013 |
| 0.21 | 0.011 | 0.027 | 0.045 | 0.109 | 0.071 | 0.012 |
| 0.22 | 0.010 | 0.026 | 0.043 | 0.105 | 0.069 | 0.012 |
| 0.23 | 0.010 | 0.025 | 0.041 | 0.102 | 0.066 | 0.011 |
| 0.24 | 0.010 | 0.024 | 0.039 | 0.098 | 0.063 | 0.011 |
| 0.25 | 0.009 | 0.023 | 0.038 | 0.095 | 0.061 | 0.010 |
| 0.26 | 0.009 | 0.022 | 0.036 | 0.091 | 0.059 | 0.010 |
| 0.27 | 0.008 | 0.021 | 0.035 | 0.088 | 0.057 | 0.009 |
| 0.28 | 0.008 | 0.020 | 0.033 | 0.085 | 0.055 | 0.009 |
| 0.29 | 0.008 | 0.019 | 0.032 | 0.083 | 0.053 | 0.008 |
| 0.30 | 0.007 | 0.019 | 0.031 | 0.080 | 0.051 | 0.008 |

Supplementary Discussion

Filtering for alteration and the composition of Archean komatiites

Due to their long residence in the crust the $\delta^{98}\text{Mo}$ of Archean komatiites may have been modified by alteration or metamorphism due to the mobility of Mo in fluids^{34,35}. Here we have used a plot of Mn/Fe^{2+} versus Al/Fe^{2+} to assess the extent of alteration in the komatiites (Fig. S1). This type of plot has been used previously to assess alteration in komatiites^{1,2}. Given that Fe and Mn have similar chemical behaviour during magmatic differentiation; olivine generally has a similar Mn/Fe^{2+} as the initial melt, therefore addition or crystallisation of olivine will not significantly fractionate Mn/Fe^{2+} . Therefore, samples that plot perpendicular to the magmatic differentiation trend must have been affected by Fe or Mn mobilization and their $\delta^{98}\text{Mo}$ values may have been modified by secondary alteration after emplacement. For the data presented previously by Greber, et al.³ the olivine-cumulates from the Weltevreden and Munro komatiites generally have more variable $\delta^{98}\text{Mo}$ than the spinifex-textured lavas at the same locations (Figs. 1 and S1); with the spinifex-texture samples falling close to the field defined by unaltered magmas undergoing magmatic differentiation. This may presumably be due to a higher proportion of easily altered olivine phenocrysts in the cumulate samples. However, there is no inherent reason why spinifex-texture samples should be less altered than cumulates, one of the spinifex-texture samples measured here has an extremely fractionated $\delta^{98}\text{Mo}$ ($422-99 = +0.007\text{‰}$) and has disturbed Mn/Fe^{2+} . Thus, exclusion for alteration needs to be done on a geochemical rather than rock type basis.

The averages presented here for the Weltevreden ($-0.215 \pm 0.038\text{‰}$) and Munro komatiites ($-0.196 \pm 0.044\text{‰}$; Table S3) have are identical within error to those calculated when including all of the Greber, et al.³ data which are $-0.206 \pm 0.071\text{‰}$ ($n = 7$) for Weltevreden and $-0.211 \pm 0.043\text{‰}$

($n = 9$) for Munro. Inclusion of the previously excluded data also makes little difference to the average composition of Archean komatiites which becomes $-0.204 \pm 0.028\text{‰}$ ($n = 20$) and remains resolvable sub-chondritic. In summary, independent of the samples used and the rationale for excluding altered samples the conclusion holds that Archean komatiites are sub-chondritic.

The Baffin Island picrites and correlations with $\delta^{98}\text{Mo}$

Although previous studies have shown that $\delta^{98}\text{Mo}$ is unaffected during anhydrous magmatic differentiation^{21,36} (see Fig. S2), the Baffin Island picrites represent a special case. The fact olivine accumulation controls the major element compositions of the Baffin Island picrites is well established^{9,37-40}. Here we show Mo concentrations of the Baffin Island samples are strongly correlated with MgO, like many other trace elements (Fig. S3). However, due to the incompatibility of Mo in olivine ($D_{\text{Mo}} = 0.006$ ²⁹), we would expect no significant effect on $\delta^{98}\text{Mo}$. Previous work by McCoy-West, et al.⁹ showed the Fe and Zn isotope compositions of individual olivines are as light as -0.8‰ for $\delta^{56}\text{Fe}$ and -0.3‰ for $\delta^{66}\text{Zn}$, with the bulk rock compositions controlled by the accumulation of variable amounts of olivine that is out of equilibrium with the melt (thus significant kinetic isotope fractionation occurred). A strong covariation between $\delta^{98}\text{Mo}$ and $\delta^{66}\text{Zn}$ (Fig. S4) suggests these variations are controlled by the same process, with correlations also seen with trace element ratios or elemental concentrations (Fig. S5). Presumably when this diffusional re-equilibration is occurring for Fe and Zn, heavy Mo isotopes were also being preferentially removed from the crystals and entering the melt (all things being equal heavy isotopes prefer the strongest bonds⁴¹; i.e. lowest coordination number; see Table S8). Olivines that have then undergone kinetic isotope exchange can then be extremely isotopically light.

Variable amounts of these unique olivines are then entrained in subsequent melts and due to the low concentration of Mo in the melt can possibly affect the bulk rock composition.

However, due to the very low Mo concentration (<0.51 ppb) in olivine mass balance calculations fail to reproduce the compositions of the olivine rich samples (e.g. PI-40) using olivine alone. An alternate scenario is additional Mo is hosted within chromite or sulfide inclusions within the olivines. Leaching experiments were conducted on two samples (see Table S5) and the non-silicate (chromite or sulfide) fraction is resolvable isotopically lighter than the residual silicate trapped Mo, this non-silicate fraction also contains $\sim 40\%$ of the Mo of the samples.

Ultimately, the exact nature of this correlation with respect to Mo isotopes is not particularly important for our purposes here. What is important is: 1) the strong linear trends versus a range of different trace element concentrations and ratios (Figs. S4 & S5) shows this is the result of linear addition (i.e. crystal accumulation) rather than magmatic differentiation (where parabolic curves would be expected); and 2) these correlations allow calculation of the composition of the Baffin Island parental melt (Table S2) which is identical within error to all of the other high temperature high degree partial melts measured from 3.5 Ga to the present (Table S3).

Estimates of the composition of Mid-ocean ridge basalts

The composition of the MORB mantle is a contentious issue in the Mo isotope scientific literature, with inconsistency between published results^{21,22,42}. Initial work by Hibbert, et al.⁴³ processed ~ 1 g of handpicked glasses and obtain $\delta^{98}\text{Mo}$ values of ca. -0.15 to -0.25% . A comprehensive study of MORB glasses by Bezard, et al.²¹ found the average composition of normal MORB was $-0.180 \pm 0.016\%$ ($n = 18$; as in the main text all errors are 95% s.e.), with the five most depleted samples representative of depleted MORB, uncontaminated by recycled crustal sediments, being slightly

sub-chondritic with a an average $\delta^{98}\text{Mo}$ of $-0.206 \pm 0.021\text{‰}$ ($n = 5$). These studies agree with the average composition of the least altered oceanic crust from ODP site 1256 reported as $-0.20 \pm 0.06\text{‰}$ ($n = 5$)⁴⁴. In stark contrast, Liang, et al.²² found an average MORB composition of $\delta^{98}\text{Mo} = +0.005 \pm 0.025\text{‰}$ ($n = 10$). Here we have reanalysed one of the MORB samples presented in Liang, et al.²² from the North Atlantic Ridge (45N; provided by Kevin Burton in both cases) that had a reported composition of $+0.03 \pm 0.07\text{‰}$. Our reanalysis produces an identical Mo concentration of 0.41 ppm, but a distinctly different $\delta^{98}\text{Mo}$ value of $-0.159 \pm 0.056\text{‰}$ ($n = 2$), which is in agreement with published values for enriched MORBs from the Mohs-Knipovich-Jan Mayen Ridge analysed by Bezard, et al.²¹ which range from -0.08 to -0.15‰ . This new analysis cast doubt over the MORB analyses presented in Liang, et al.²². Therefore, in this work we use the published MORB data presented in Bezard, et al.²¹. Emphasis here has been placed on the composition of the depleted MORB mantle because a range isotopic studies⁴⁵⁻⁴⁷ have shown the majority of MORB samples are contaminated by recycled sedimentary material.

The composition of the endmembers used in crustal estimate calculations

Modern crustal values of $\delta^{98}\text{Mo}$ and $[\text{Mo}]$ are probably not representative of the composition of the early proto-crust, hence here we have modelled a range of crust types using the best estimates of Archean compositions available. The composition of Archean crust can never be determined with certainty, because of the poor preservation of such old rocks⁴⁸. Indirect approaches, however, suggest the crust was probably dominantly mafic in composition with a subordinate amount of felsic rocks e.g.^{48,49,50-52}. Following this idea, we created 3 different compositions of Archean crust by mixing different amount of felsic and mafic rocks- purely felsic, intermediate and dominantly-mafic, which would fully encompass its compositional uncertainty. Clearly the first one is

hypothetical, and the latter two are more representative of the Archean crust. For mass balance calculations, we needed two values- elemental, [Mo] and isotopic, $\delta^{98}\text{Mo}$ composition of Mo for the felsic and mafic counterparts (i.e., total four parameters):

1) Only [Mo] of Archean felsic rocks (TTGs and granites) are available ¹⁴ which we have used. For all the other parameters, we needed proxies.

2) The [Mo] of the basalt endmember (0.155) has been model based on partial melting of the mantle by 30% (sitting in the middle of the Archean range; ^{18,19}) to produce a high Mg basalt using well constrained D values; ^{16,29}. Due to the incompatible nature of Mo, varying the degree of melting from 20 to 40% does not substantial change this value it from 0.23 to 0.12 ppm (Fig. S9).

3) We chose the $\delta^{98}\text{Mo}$ of average modern basalts (-0.10‰) to represent the mafic endmember. The partial melting model presented in Figure 3 shows that melting of a chondritic mantle reservoir to form basalt would reproduce this value with $\sim 12\%$ melting at 1300 °C . This $\sim 0.05\text{ ‰}$ offset is comparable to the natural offset observed between N-MORB ²¹ and the accessible mantle herein. Melting at higher temperatures or greater degrees of melting would result in a lighter melt. Changing of the composition of the basalt to -0.12‰ results in a difference in V_{PCC} of only 0.12 (for the 50:50 model at 30% mantle depletion), which is smaller than the already displayed error envelopes based on varying endmember composition (see Fig. 4).

4) Archean felsic rocks are dominated by TTGs with rare granites (see ⁵³ for a review). TTGs are chemically evolved rocks ($\text{SiO}_2 > 65\%$) like granites, but they are primarily characterized by higher Na/K values than true granites. For our purpose, it is important to see what the likely difference in $\delta^{98}\text{Mo}$ between Archean TTGs and modern granites. The elemental concentration of Mo in TTGs and modern and Archean granites are plotted in Figure S7. Phanerozoic granites (Av. Mo = 0.90 ppm) have significantly higher [Mo] than Archean TTGs (Av Mo = 0.28 ppm). Presumably

because granites are the result of the multiple episodes of reworking. Therefore, in Figure 4 we present two endmember models, a granite model which provides minimum values of crustal volume and uses the $\delta^{98}\text{Mo}$ of modern granites (+0.16‰) and a TTG model which provides the most realistic estimate of the volumes of early crust based on the available information. Given that TTGs have lower Mo concentrations than granites it is sensible to assume their $\delta^{98}\text{Mo}$ will also be less evolved. Here we have taken the simplest approach (i.e. two step formation of TTGs) and taken the average of global basalts and granites to estimate the $\delta^{98}\text{Mo}$ of TTG felsic component (+0.03‰). This intermediate composition of TTGs is confirmed by Zn isotope analyses these rock types ⁵⁴.

There is no *a priori* reason to assume that partial melting processes were different in the Archean than they are today. Therefore, we do not expect significant uncertainties in the crustal volume presented in this study due to the lack of exact match between our chosen proxies for Archean crust and the real Archean crust.

The effect of partial melting on Mo isotopes

Two major factors, redox and co-ordination, will control the fractionation of Mo stable isotopes during partial melting e.g. ⁴¹. Due to the oxidised nature of the terrestrial upper mantle ($\approx\text{FMQ}$), in partial melts of this mantle, Mo predominantly occurs as tetrahedral co-ordinated Mo^{6+} (MoO_4^{2-}) ^{30,55}. Furthermore, given Mo^{6+} is significantly more incompatible than Mo^{4+} ²⁹ melting products will have higher $\text{Mo}^{6+}/\Sigma\text{Mo}$ than their residue, and hence will be heavier. Co-ordination is a subordinate effect but will also result in an isotopically heavy melt, with Mo in pyroxene (octahedral; ⁵⁶) and olivine having higher co-ordination than in the melt, with heavy isotopes preferentially moving to sites with the lowest coordination number ⁴¹. The generation of

isotopically heavy melts is consistent with the fact average global basalt ($\delta^{98}\text{Mo} = -0.10 \pm 0.04\text{‰}$; ¹⁵), are isotopically heavier than the bulk accessible mantle we observe today ($\delta^{98}\text{Mo} = -0.20 \pm 0.01\text{‰}$; see Table S3). Because Mo is highly incompatible during mantle melting $D_{\text{Mo}} = 0.006\text{--}0.008$ ^{16,29}, it will be quantitatively extracted into the melt except at low degrees of melting (see Fig. S9).

Here we have constructed a non-modal batch melting to show the fractionation of Mo isotopes during partial melting based upon the general principles outlined in Sossi and O'Neill ³³ (See Fig. 3). This model uses the Born-Mayer repulsion approximation to calculate force constants that has been shown to be adequate for other condensed phases ^{33,57,58}. The model set up and parameters used in modelling are described in Table S7 and Table S8. The predominant oxidation state of Mo on Earth ^{29,30,55,59}, Mo^{6+} is VI-fold (octahedral) co-ordinated in minerals^{55,56} and predominantly IV-fold (tetrahedral) in silicate melts ³⁰. Literature reports suggest that Mo^{4+} exists in octahedral co-ordination ($^{\text{VI}}\text{Mo}$) both in minerals and melts, due to a lack of stability of the hypothetical $^{\text{IV}}\text{Mo}^{4+}$ compound ^{30,32}. Here we have used the measured Mo-O bond lengths ³⁰⁻³² to calculate the force constants reported in Table S8 and Figure S10. These values have been confirmed as accurate using the Shannon Radius approximation. Where the mean Mo-O bond distance is the sum of the Shannon ionic radius for these species in the appropriate co-ordination environment and that of O^{2-} (1.38 Å).

At high degrees of melting as observed in komatiites and the Baffin Island picrites (20-40 % melting), they will remain essential unfractionated from their source region due to the complete removal of Mo from their residue (Fig. 3; Table S9). The corollary is that any Mo remaining in the residual mantle after partial melting is isotopically lighter. At smaller degrees of melting or more reduced conditions the $\Delta^{98}\text{Mo}_{\text{melt-residue}}$ can be larger.

On the modern Earth Mo occurs predominantly Mo^{6+} ^{29,30,55,59} ($\text{Mo}^{6+}/\Sigma\text{Mo} \approx 0.99$), however, it is possible that previous period in Earth's history the mantle may have been more reduced, which would result in the generation of isotopically heavier melts ($\Delta^{98}\text{Mo}_{\text{melt-solid}} > 0.1\text{‰}$; Fig. 3b; S10). The work of Nicklas et al. ^{60,61} suggests there was a secular increase in upper mantle oxygen fugacity from 3.5 to 2.4 Ga, providing an upper bound on oxygen fugacity prior to 3.5 Ga (Using Fig. 5 in ⁶¹ oxidation fugacity could be as low as $\Delta\text{FMQ} = -0.5$). O'Neill and Eggins ⁵⁵ show minimal Mo^{4+} at FMQ but demonstrate that there is a strong compositional dependence on this relationship. Using Figure 10 in ⁵⁵ and the MAS2 composition (25 wt% MgO as expected in the early Earth melting conditions) and using this lower bound at 3.5 Ga of $\Delta\text{FMQ} = -0.5$ ^{60,61} we calculate a $\text{Mo}^{6+}/\Sigma\text{Mo} \approx 0.95$, which is adopted in the temperature dependent modelling presented in Figure 3.

It has also been suggested based on stable isotope evidence that the Earth and Moon equilibrated during the Moon forming impact ^{42,62,63}. The lunar mantle has an oxygen fugacity of ca. IW-1 and thus Earth's mantle may have experienced a short period at more reduced conditions. We have included modelling at highly reduced conditions (See Fig. S11, Table S10) because it is relevant to melting processes on other celestial bodies (e.g. Moon, Angrites), we are not advocating that the Earth's mantle is currently at these highly reduced conditions.

Alternative estimates of the composition of the bulk silicate Earth

In the main text we have assumed the Mo isotope composition of the bulk silicate Earth (BSE) is the same as the chondritic meteorites Earth accreted from ($\delta^{98}\text{Mo} = -0.154 \pm 0.013\text{‰}$; ^{22,23}). Here we investigate the effects of alternate scenarios on the volume of crust extraction required in the early Earth: 1) the Mo isotope composition of BSE was modified during core formation; or 2) the composition of the BSE is the same as the bulk silicate Moon.

Modification during core formation (Model 2): The near quantitative removal of Mo to the metallic core means the metallic phase is unlikely to be fractionated from bulk chondrites, as is observed in iron meteorites ²³. However, this sequestration of Mo may have been associated with a small but resolvable isotopic fractionation of the silicate portion of the planet of up to 0.3‰ ²³. When extrapolating to temperatures more closely approximating core formation (>2000 °C ⁶⁴) initial metal-silicate equilibration experiments ⁶⁵ suggested a resolvable $\Delta^{98}\text{Mo}_{\text{metal-silicate}}$ of -0.052‰ at 2500 °C, but subsequent work which incorporates the effect of Mo valance state ⁵⁹ suggests a significantly reduced $\Delta^{98}\text{Mo}_{\text{metal-silicate}}$ of as little as -0.008‰ (assuming reduced conditions with $\text{Mo}^{6+}/\Sigma\text{Mo} = 0.1$). This parameterization requires accurate knowledge of both the temperature and oxygen fugacity at the time of core formation, neither of which we know with certainty. However, we can make an educated estimate on the maximum effect of core formation. Core formation is expected to occur between 2000 °C and 3000 °C ^{64,66-68} and requires highly reduced conditions initially ^{64,69}. A reasonable upper estimate of the maximum effect of core formation could impart is $\Delta^{98}\text{Mo}_{\text{metal-silicate}} = -0.012\text{‰}$ (assuming $T = 2000\text{ °C}$; $\text{Mo}^{6+}/\Sigma\text{Mo} = 0.1$), meaning that if the mantle is indeed isotopically heavier it will still be within error of the composition of chondrites. Crustal volume estimates based on an isotopically heavier BSE following core formation ($\delta^{98}\text{Mo} = -0.142\text{‰}$) are presented in Figure S6 (c-d). These estimates are higher (3.4-5.3 times PVCC) but not drastically different than the modelling assuming a chondritic BSE.

Composition similar to bulk silicate Moon (Model 3): We also explored the effect of a BSE composition based on the Earth-Moon equilibration as done by Willbold and Elliott ⁴². This idea is based on assuming the BSE and Moon were once isotopically equilibrated as has been shown for several lithophile elements ^{62,63}. Using analyses of lunar samples ($\delta^{98}\text{Mo} = -0.050 \pm 0.033\text{‰}$;

²³), and assuming subsequent late accretion of 1% chondritic material results in a $\delta^{98}\text{Mo}$ of -0.078‰ . By using this value for the BSE and then undertaking mass balance modelling to investigate the volume of crust, generates unrealistically large volumes of crust (Fig. S6e-f). Namely, using TTG felsic materials for mafic crust-A (50:50 mafic-felsic rocks) and a depleted mantle comprising 30% of the mantle would require 14 times the PVCC. This value is even higher for the mafic crust-B (75:25 mafic-felsic rocks). Requiring >10 times the PVCC is highly unrealistic, considering the recycling rates and present extent of crustal volume. Therefore, for Mo it is extremely unlikely that the BSE was ever fully equilibrated with the bulk silicate Moon.

The effect of the lower crust

On the modern Earth the continental crust has a well-developed lower crust ⁴⁸⁻⁵⁰. Estimates of the composition of the continental crust from molybdenites, granites and arc-related basalts are consistent with a super-chondritic $\delta^{98}\text{Mo}$ from $+0.05$ to $+0.30\text{‰}$ ^{15,70,71}. These archives are focused on the upper continental crust (arc basalts are a record of juvenile continental crust), but do not consider the effect of possible compositional variations in the lower crust. However, given the extreme incompatibility of Mo during mantle melting $D_{\text{Mo}} = 0.006-0.008$ ^{16,29}, Mo essentially becomes concentrated in the upper crust rather than any lower crustal cumulates. An additional complication would be the presence of residual sulfides, that due to its chalcophile behaviour will preferentially incorporate Mo. However, given on the modern Earth most continental crust is predominantly formed in subduction-like environments sulfide-saturation will generally be delayed (due to higher $f\text{O}_2$, and water contents), and therefore Mo will remain in the melt phase and removed to the upper crust.

The composition and makeup of the Archean crust was not identical to modern crust ⁴⁸⁻⁵⁰. Therefore, whether the Archean crust has a well-defined lower crust similar to today or not is unknown. Instead, studies infer that the whole Archean crust was dominantly mafic and may have contained subordinate amount of granitoids ^{49,51,52}. We have considered this factor while carrying out the mass balance modelling by using 3 different crustal compositions: (1) purely felsic (100% granitoids); (2) intermediate (Mafic crust-A; combination of mafic-felsic in 50:50); and (3) dominantly-mafic (Mafic crust-B; with a mafic-felsic ratio of 75:25). The mafic component of the latter two crustal types is approximated from the Mo isotope composition of global average of basalts (juvenile melt). Now, TTGs form when these basalts get metamorphosed and partially melted at amphibolite or eclogite facies e.g. ^{72,73}. Therefore, we should expect a depleted residual mass in the lower crust complementing the TTG composition. But, this depleted lower crust is extremely unlikely to remain preserved in the crust, due to the geodynamic setting where Hadean to early Archean TTGs are inferred to have formed (i.e. a stagnant-lid regime: either when the meta-basalts drip back into the mantle (delamination) or during the mantle lid overturn events that recycle the pre-existing crust back to the mantle ^{53,73-75}). The crucial point is, the preserved crustal profile is largely devoid of residues formed after TTG extraction. Therefore, the crust is dominated by juvenile, melt-undepleted (meta-)basalts and granitoids. As stated above, our existing mass balance calculations consider both these components of the Archean crust as realistically as possible. Furthermore, even if some fraction of this TTG-depleted residual mass remains in the crust, it is likely to be of granulite to eclogite grade- where rutile exists ⁷². It has been shown that in such cases, rutile should dominate the Mo-budget ^{14,76,77}. Mo-concentration within such eclogitic rutile can vary within 2-7 ppm ⁷⁷ and thermodynamic phase equilibria modelling suggests that the Archean meta-basalts would have contained not more than ~0.5 volume % of rutile ⁷⁸. In that case,

the net Mo concentration will not deviate much from that of average basalt, which we have already considered for the mafic component of our model crustal types. This further attest that the crustal volume range bracketed by the intermediate and dominantly-mafic crustal types potentially accounts for the variations due to any depleted lower crustal rocks.

References

- 1 Hibbert, K. E. J., Williams, H. M., Kerr, A. C. & Puchtel, I. S. Iron isotopes in ancient and modern komatiites: Evidence in support of an oxidised mantle from Archean to present. *Earth and Planetary Science Letters* **321–322**, 198–207, doi:10.1016/j.epsl.2012.01.011 (2012).
- 2 Dauphas, N., Teng, F.-Z. & Arndt, N. T. Magnesium and iron isotopes in 2.7 Ga Alexo komatiites: Mantle signatures, no evidence for Soret diffusion, and identification of diffusive transport in zoned olivine. *Geochimica et Cosmochimica Acta* **74**, 3274–3291, doi:10.1016/j.gca.2010.02.031 (2010).
- 3 Greber, N. D., Puchtel, I. S., Nägler, T. F. & Mezger, K. Komatiites constrain molybdenum isotope composition of the Earth's mantle. *Earth and Planetary Science Letters* **421**, 129–138, doi:10.1016/j.epsl.2015.03.051 (2015).
- 4 Puchtel, I. S., Humayun, M., Campbell, A. J., Sproule, R. A. & Leshner, C. M. Platinum group element geochemistry of komatiites from the Alexo and Pyke Hill areas, Ontario, Canada 11 Associate editor: R. J. Walker. *Geochimica et Cosmochimica Acta* **68**, 1361–1383, doi:10.1016/j.gca.2003.09.013 (2004).
- 5 Puchtel, I. S. *et al.* Insights into early Earth from Barberton komatiites: Evidence from lithophile isotope and trace element systematics. *Geochimica et Cosmochimica Acta* **108**, 63–90, doi:10.1016/j.gca.2013.01.016 (2013).
- 6 Starkey, N. A. *et al.* Helium isotopes in early Iceland plume picrites: Constraints on the composition of high $^3\text{He}/^4\text{He}$ mantle. *Earth and Planetary Science Letters* **277**, 91–100, doi:10.1016/j.epsl.2008.10.007 (2009).
- 7 Sossi, P. A. *et al.* Petrogenesis and Geochemistry of Archean Komatiites. *Journal of Petrology* **57**, 147–184, doi:10.1093/petrology/egw004 (2016).
- 8 Kerr, A. C. La Isla de Gorgona, Colombia: A petrological enigma? *Lithos* **84**, 77–101, doi:10.1016/j.lithos.2005.02.006 (2005).
- 9 McCoy-West, A. J., Godfrey Fitton, J., Pons, M.-L., Inglis, E. C. & Williams, H. M. The Fe and Zn isotope composition of deep mantle source regions: Insights from Baffin Island picrites. *Geochimica et Cosmochimica Acta* **238**, 542–562, doi:10.1016/j.gca.2018.07.021 (2018).
- 10 Jacobsen, S. B. Isotopic and chemical constraints on mantle-crust evolution. *Geochimica et Cosmochimica Acta* **52**, 1341–1350, doi:10.1016/0016-7037(88)90205-0 (1988).
- 11 DePaolo, D. J. Crustal growth and mantle evolution: inferences from models of element transport and Nd and Sr isotopes. *Geochimica et Cosmochimica Acta* **44**, 1185–1196, doi:10.1016/0016-7037(80)90072-1 (1980).
- 12 Jacobsen, S. B. & Wasserburg, G. J. The mean age of mantle and crustal reservoirs. *Journal of Geophysical Research: Solid Earth* **84**, 7411–7427, doi:10.1029/JB084iB13p07411 (1979).
- 13 O'Nions, R. K., Evensen, N. M. & Hamilton, P. J. Geochemical modeling of mantle differentiation and crustal growth. *Journal of Geophysical Research: Solid Earth* **84**, 6091–6101, doi:10.1029/JB084iB11p06091 (1979).
- 14 Greaney, A. T. *et al.* Geochemistry of molybdenum in the continental crust. *Geochimica et Cosmochimica Acta* **238**, 36–54, doi:10.1016/j.gca.2018.06.039 (2018).
- 15 Yang, J. *et al.* The molybdenum isotopic compositions of I-, S- and A-type granitic suites. *Geochimica et Cosmochimica Acta* **205**, 168–186, doi:10.1016/j.gca.2017.01.027 (2017).
- 16 Wang, Z. & Becker, H. Molybdenum partitioning behavior and content in the depleted mantle: Insights from Balmuccia and Baldissero mantle tectonites (Ivrea Zone, Italian Alps). *Chemical Geology* **499**, 138–150, doi:10.1016/j.chemgeo.2018.09.023 (2018).
- 17 Palme, H. & O'Neill, H. S. C. in *Treatise on Geochemistry (Second Edition)* (eds Heinrich D. Holland & Karl K. Turekian) 1–39 (Elsevier, 2014).
- 18 Herzberg, C., Condie, K. & Korenaga, J. Thermal history of the Earth and its petrological expression. *Earth and Planetary Science Letters* **292**, 79–88, doi:10.1016/j.epsl.2010.01.022 (2010).
- 19 Keller, C. B. & Schoene, B. Statistical geochemistry reveals disruption in secular lithospheric evolution about 2.5 Gyr ago. *Nature* **485**, 490, doi:10.1038/nature11024 (2012).
- 20 Isoplot 3.71 v. 3.71 (Berkeley Geochronology Centre, 2008).
- 21 Bezard, R., Fischer-Gödde, M., Hamelin, C., Brennecka, G. A. & Kleine, T. The effects of magmatic processes and crustal recycling on the molybdenum stable isotopic composition of Mid-Ocean Ridge Basalts. *Earth and Planetary Science Letters* **453**, 171–181, doi:10.1016/j.epsl.2016.07.056 (2016).
- 22 Liang, Y.-H. *et al.* Molybdenum isotope fractionation in the mantle. *Geochimica et Cosmochimica Acta* **199**, 91–111, doi:10.1016/j.gca.2016.11.023 (2017).

- 23 Burkhardt, C., Hin, R. C., Kleine, T. & Bourdon, B. Evidence for Mo isotope fractionation in the solar nebula and during planetary differentiation. *Earth and Planetary Science Letters* **391**, 201-211, doi:10.1016/j.epsl.2014.01.037 (2014).
- 24 Yoder, C. F. in *Global Earth Physics: A Handbook of Physical Constants* Vol. AGU Reference Shelf (ed T. J. Ahrens) pp. 1–31 (American Geophysical Union, 1995).
- 25 McDonough, W. F. in *Treatise on Geochemistry (First Edition)* Vol. 2 (eds Heinrich D. Holland & Karl K. Turekian) 547-568 (Elsevier, 2003).
- 26 Salters, V. J. M. & Stracke, A. Composition of the depleted mantle. *Geochemistry, Geophysics, Geosystems* **5**, doi:doi:10.1029/2003GC000597 (2004).
- 27 Rudnick, R. L. & Gao, S. in *Treatise on Geochemistry (Second Edition)* (eds Heinrich D. Holland & Karl K. Turekian) 1-51 (Elsevier, 2014).
- 28 Walter, M. J. in *Treatise of Geochemistry* Vol. 2.08 (ed R. W. Carlson) 363-394 (Elsevier, 2003).
- 29 Leitzke, F. P. *et al.* Redox dependent behaviour of molybdenum during magmatic processes in the terrestrial and lunar mantle: Implications for the Mo/W of the bulk silicate Moon. *Earth and Planetary Science Letters* **474**, 503-515, doi:10.1016/j.epsl.2017.07.009 (2017).
- 30 Farges, F. o., Siewert, R., Brown, J. G. E., Guesdon, A. & Morin, G. Structural environments around molybdenum in silicate glasses and melts. I. Influence of composition and oxygen fugacity on the local structure of molybdenum. *The Canadian Mineralogist* **44**, 731-753, doi:10.2113/gscanmin.44.3.731 (2006).
- 31 Kihlberg, L. Least squares refinement of the crystal structure of molybdenum trioxide. *Arkiv för Kemi* **21**, 357-364 (1963).
- 32 Brandt, B. G. & Skapski, A. C. A refinement of the crystal structure of molybdenum dioxide. *Acta Chemica Scandinavica* **21**, 661-672 (1967).
- 33 Sossi, P. A. & O'Neill, H. S. C. The effect of bonding environment on iron isotope fractionation between minerals at high temperature. *Geochimica et Cosmochimica Acta* **196**, 121-143, doi:10.1016/j.gca.2016.09.017 (2017).
- 34 Bali, E., Keppler, H. & Audetat, A. The mobility of W and Mo in subduction zone fluids and the Mo–W–Th–U systematics of island arc magmas. *Earth and Planetary Science Letters* **351–352**, 195-207, doi:10.1016/j.epsl.2012.07.032 (2012).
- 35 Keppler, H. & Wyllie, P. J. Partitioning of Cu, Sn, Mo, W, U, and Th between melt and aqueous fluid in the systems haplogranite-H₂O–HCl and haplogranite-H₂O–HF. *Contributions to Mineralogy and Petrology* **109**, 139-150, doi:10.1007/bf00306474 (1991).
- 36 Yang, J. *et al.* Absence of molybdenum isotope fractionation during magmatic differentiation at Hekla volcano, Iceland. *Geochimica et Cosmochimica Acta* **162**, 126-136, doi:10.1016/j.gca.2015.04.011 (2015).
- 37 Clarke, D. B. Tertiary basalts of Baffin Bay: Possible primary magma from the mantle. *Contributions to Mineralogy and Petrology* **25**, 203-224, doi:10.1007/bf00371131 (1970).
- 38 Francis, D. The Baffin Bay lavas and the value of picrites as analogues of primary magmas. *Contributions to Mineralogy and Petrology* **89**, 144-154, doi:10.1007/BF00379449 (1985).
- 39 Larsen, L. M. & Pedersen, A. K. Processes in high-Mg, high-T magmas: Evidence from olivine, chromite and glass in Palaeogene picrites from West Greenland. *Journal of Petrology* **41**, 1071-1098, doi:10.1093/petrology/41.7.1071 (2000).
- 40 Starkey, N. A., Fitton, J. G., Stuart, F. M. & Larsen, L. M. Melt inclusions in olivines from early Iceland plume picrites support high ³He/⁴He in both enriched and depleted mantle. *Chemical Geology* **306–307**, 54-62, doi:10.1016/j.chemgeo.2012.02.022 (2012).
- 41 Schauble, E. A. Applying Stable Isotope Fractionation Theory to New Systems. *Reviews in Mineralogy and Geochemistry* **55**, 65-111 (2004).
- 42 Willbold, M. & Elliott, T. Molybdenum isotope variations in magmatic rocks. *Chemical Geology* **449**, 253-268, doi:10.1016/j.chemgeo.2016.12.011 (2017).
- 43 Hibbert, K., Freymuth, H., Willbold, M. & Elliott, T. Mass-dependent molybdenum isotopes in mid-ocean ridge basalts: A new mantle reference. *American Geophysical Union Fall Meeting San Francisco, California*, Abstract V52A-04 (2013).
- 44 Freymuth, H., Vils, F., Willbold, M., Taylor, R. N. & Elliott, T. Molybdenum mobility and isotopic fractionation during subduction at the Mariana arc. *Earth and Planetary Science Letters* **432**, 176-186, doi:10.1016/j.epsl.2015.10.006 (2015).
- 45 Nielsen, S. G. *et al.* Barium isotope evidence for pervasive sediment recycling in the upper mantle. *Science Advances* **4**, doi:10.1126/sciadv.aas8675 (2018).

- Andersen, M. B. *et al.* The terrestrial uranium isotope cycle. *Nature* **517**, 356, doi:10.1038/nature14062 (2015).
- Rehkamper, M. & Hofmann, A. W. Recycled ocean crust and sediment in Indian Ocean MORB. *Earth and Planetary Science Letters* **147**, 93-106, doi:10.1016/S0012-821X(97)00009-5 (1997).
- Cawood, P. A., Hawkesworth, C. J. & Dhuime, B. The continental record and the generation of continental crust. *GSA Bulletin* **125**, 14-32, doi:10.1130/B30722.1 (2013).
- Kamber, B. S., Whitehouse, M. J., Bolhar, R. & Moorbath, S. Volcanic resurfacing and the early terrestrial crust: Zircon U–Pb and REE constraints from the Isua Greenstone Belt, southern West Greenland. *Earth and Planetary Science Letters* **240**, 276-290, doi:10.1016/j.epsl.2005.09.037 (2005).
- Cawood, P. A. *et al.* Geological archive of the onset of plate tectonics. *Philosophical Transactions of the Royal Society A: Mathematical, Physical and Engineering Sciences* **376**, 20170405, doi:10.1098/rsta.2017.0405 (2018).
- Dhuime, B., Wuestefeld, A. & Hawkesworth, C. J. Emergence of modern continental crust about 3 billion years ago. *Nature Geoscience* **8**, 552, doi:10.1038/ngeo2466 (2015).
- Tang, M., Chen, K. & Rudnick, R. L. Archean upper crust transition from mafic to felsic marks the onset of plate tectonics. *Science* **351**, 372-375, doi:10.1126/science.aad5513 (2016).
- Moyen, J.-F. & Laurent, O. Archean tectonic systems: A view from igneous rocks. *Lithos* **302-303**, 99-125, doi:10.1016/j.lithos.2017.11.038 (2018).
- Doucet, L. S., Laurent, O., Mattielli, N. & Debouge, W. Zn isotope heterogeneity in the continental lithosphere: New evidence from Archean granitoids of the northern Kaapvaal craton, South Africa. *Chemical Geology* **476**, 260-271, doi:10.1016/j.chemgeo.2017.11.022 (2018).
- O'Neill, H. S. C. & Eggins, S. M. The effect of melt composition on trace element partitioning: an experimental investigation of the activity coefficients of FeO, NiO, CoO, MoO₂ and MoO₃ in silicate melts. *Chemical Geology* **186**, 151-181, doi:10.1016/S0009-2541(01)00414-4 (2002).
- Adam, J. & Green, T. Trace element partitioning between mica- and amphibole-bearing garnet lherzolite and hydrous basanitic melt: 1. Experimental results and the investigation of controls on partitioning behaviour. *Contributions to Mineralogy and Petrology* **152**, 1-17, doi:10.1007/s00410-006-0085-4 (2006).
- Bourdon, B., Roskosz, M. & Hin, R. C. Isotope tracers of core formation. *Earth-Science Reviews* **181**, 61-81, doi:10.1016/j.earscirev.2018.04.006 (2018).
- Young, E. D. *et al.* High-temperature equilibrium isotope fractionation of non-traditional stable isotopes: Experiments, theory, and applications. *Chemical Geology* **395**, 176-195, doi:10.1016/j.chemgeo.2014.12.013 (2015).
- Hin, R. C., Burnham, A. D., Gianolio, D., Walter, M. J. & Elliott, T. Molybdenum isotope fractionation between Mo⁴⁺ and Mo⁶⁺ in silicate liquid and metallic Mo. *Chemical Geology* **504**, 177-189, doi:10.1016/j.chemgeo.2018.11.014 (2019).
- Nicklas, R. W., Puchtel, I. S. & Ash, R. D. Redox state of the Archean mantle: Evidence from V partitioning in 3.5–2.4 Ga komatiites. *Geochimica et Cosmochimica Acta* **222**, 447-466, doi:10.1016/j.gca.2017.11.002 (2018).
- Nicklas, R. W. *et al.* Secular mantle oxidation across the Archean-Proterozoic boundary: Evidence from V partitioning in komatiites and picrites. *Geochimica et Cosmochimica Acta* **250**, 49-75, doi:10.1016/j.gca.2019.01.037 (2019).
- Armstrong, R. M. G., Georg, R. B., Williams, H. M. & Halliday, A. N. Silicon isotopes in lunar rocks: Implications for the Moon's formation and the early history of the Earth. *Geochimica et Cosmochimica Acta* **77**, 504-514, doi:10.1016/j.gca.2011.10.032 (2012).
- Young, E. D. *et al.* Oxygen isotopic evidence for vigorous mixing during the Moon-forming giant impact. *Science* **351**, 493, doi:10.1126/science.aad0525 (2016).
- Wade, J. & Wood, B. J. Core formation and the oxidation state of the Earth. *Earth and Planetary Science Letters* **236**, 78-95, doi:10.1016/j.epsl.2005.05.017 (2005).
- Hin, R. C., Burkhardt, C., Schmidt, M. W., Bourdon, B. & Kleine, T. Experimental evidence for Mo isotope fractionation between metal and silicate liquids. *Earth and Planetary Science Letters* **379**, 38-48, doi:10.1016/j.epsl.2013.08.003 (2013).
- Siebert, J., Corgne, A. & Ryerson, F. J. Systematics of metal–silicate partitioning for many siderophile elements applied to Earth's core formation. *Geochimica et Cosmochimica Acta* **75**, 1451-1489, doi:10.1016/j.gca.2010.12.013 (2011).
- Righter, K., Pando, K. M., Danielson, L. & Lee, C.-T. Partitioning of Mo, P and other siderophile elements (Cu, Ga, Sn, Ni, Co, Cr, Mn, V, and W) between metal and silicate melt as a function of temperature and

- silicate melt composition. *Earth and Planetary Science Letters* **291**, 1-9, doi:10.1016/j.epsl.2009.12.018 (2010).
- 68 Ballhaus, C. *et al.* The U/Pb ratio of the Earth's mantle—A signature of late volatile addition. *Earth and Planetary Science Letters* **362**, 237-245, doi:10.1016/j.epsl.2012.11.049 (2013).
- 69 Wade, J., Wood, B. J. & Tuff, J. Metal–silicate partitioning of Mo and W at high pressures and temperatures: Evidence for late accretion of sulphur to the Earth. *Geochimica et Cosmochimica Acta* **85**, 58-74, doi:10.1016/j.gca.2012.01.010 (2012).
- 70 Voegelin, A. R., Pettke, T., Greber, N. D., von Niederhäusern, B. & Nägler, T. F. Magma differentiation fractionates Mo isotope ratios: Evidence from the Kos Plateau Tuff (Aegean Arc). *Lithos* **190–191**, 440-448, doi:10.1016/j.lithos.2013.12.016 (2014).
- 71 Greber, N. D., Pettke, T. & Nägler, T. F. Magmatic–hydrothermal molybdenum isotope fractionation and its relevance to the igneous crustal signature. *Lithos* **190–191**, 104-110, doi:10.1016/j.lithos.2013.11.006 (2014).
- 72 Moyen, J.-F. & Martin, H. Forty years of TTG research. *Lithos* **148**, 312-336, doi:10.1016/j.lithos.2012.06.010 (2012).
- 73 Johnson, T. E., Brown, M., Gardiner, N. J., Kirkland, C. L. & Smithies, R. H. Earth's first stable continents did not form by subduction. *Nature* **543**, 239, doi:10.1038/nature21383 (2017).
- 74 Sizova, E., Gerya, T., Stüwe, K. & Brown, M. Generation of felsic crust in the Archean: A geodynamic modeling perspective. *Precambrian Research* **271**, 198-224, doi:10.1016/j.precamres.2015.10.005 (2015).
- 75 Rozel, A. B., Golabek, G. J., Jain, C., Tackley, P. J. & Gerya, T. Continental crust formation on early Earth controlled by intrusive magmatism. *Nature* **545**, 332, doi:10.1038/nature22042 (2017).
- 76 Fitton, J. G. Coupled molybdenum and niobium depletion in continental basalts. *Earth and Planetary Science Letters* **136**, 715-721, doi:10.1016/0012-821X(95)00171-8 (1995).
- 77 Zack, T., Kronz, A., Foley, S. F. & Rivers, T. Trace element abundances in rutiles from eclogites and associated garnet mica schists. *Chemical Geology* **184**, 97-122, doi:10.1016/S0009-2541(01)00357-6 (2002).
- 78 Johnson, T. E., Brown, M., Kaus, B. J. P. & VanTongeren, J. A. Delamination and recycling of Archaean crust caused by gravitational instabilities. *Nature Geoscience* **7**, 47, doi:10.1038/ngeo2019 (2013).